order to monitor tail current amplitude. KCNH2/KCNE1-encoded currents were elicited by depolarizing pulses from a holding potential of −80 mV to test potentials between −60 to +50 mV (with a 10-mV step increment), before being repolarized to −60 mV in order to monitor tail current amplitude. Current densities (pA/pF) were calculated for each cell studied, by normalizing peak tail current amplitude to cell capacitance (Cm). The Cm was calculated by fitting a single exponential function to the decay phase of the transient capacitive current in response to ± 5 mV voltage steps (20 ms) from a holding potential of −50 mV. The liquid junction potential between the test solution and the pipette solution was measured as approximately −10 mV and was corrected. Data were collected and analyzed using the Patch master and Igor Pro (WaveMetrics, Lake Oswego, Oregon).

Data analyses. The voltage-dependence of current activation was determined by fitting the normalized tail current (Itail) versus test potential (Vtest) to Boltzmann's function, which is expressed by: $Itail = 1/(1 + \exp[(V_{0.5} - Vt)/k])$, where $V_{0.5}$ is the voltage at which the current is half-activated and k is the slope factor. Time constants for deactivation (τ_{fast} and τ_{slow}) were obtained by fitting a 2-exponential function to the time course of the deactivating tail currents. All data are expressed as mean ± standard error. Statistical comparisons were made using analysis of variance, followed by a *t* test, and differences were considered significant at a value of $p < 0.05$.

Results

Clinical characteristics and genotyping. Of the 496 control volunteers, 8 (mean QTc 420.5 ± 7.5 ms) had heterozygous D85N genotypes (allele frequency 0.81%). In contrast, 23 of the 317 LQTS probands had heterozygous D85N genotypes and 1 (Table 1) (Patient #24) had a homozygous D85N genotype (allele frequency 3.9%). Table 1 and Figure 1 summarize the demographics of the 24 index patients. Their mean age was 34.8 ± 4.4 years, and their mean QTc was 507.9 ± 9.2 ms. Among the D85N-negative cases, we identified 116 probands that were positive for other LQTS-related gene mutations (Fig. 1), and their mean QTc was significantly longer (540.6 ± 6.1 ms) than those of the 24 D85N carriers ($p < 0.05$).

Seven of the 23 heterozygous probands (30%) had other LQTS-related gene variants (KCNQ1 or KCNH2), and 3 female patients (13%; Patients #1, #6, and #10) had documented predisposing factors, such as electrolyte disturbances, QT prolonging drug intake, or bradycardia (Table 1). The allele frequency of the remaining 13 patients (2.1%) was significantly higher than that in the control subjects ($p < 0.05$). Six of these 13 patients (46%) had syncope and/or TdP while 9 of 10 patients (90%) with multiple genetic variants or triggering factors were symptomatic (Fig. 1).

The mean onset age of the 6 symptomatic heterozygous D85N carriers without compromised factors to affect QT

Table 1 Clinical Characteristics of the LQTS Probands Who Carried the KCNE1-D85N Variant

Patient #	Age (F/M)	QTc (ms)	Syncope	TdP	Compound Variant	Underlying Predisposing Triggers
1	36 (F)	540	+	+		Drug (bromocriptine), hypokalemia
2	9 (M)	478	−	−		
3	21 (F)	533	−	+	KCNH2 (a, S706F)*	Drug (amphetamine), hypokalemia
4	42 (F)	650	+	+		
5	51 (F)	490	+	+	KCNH2 (a, E58K)	Sinus bradycardia
6	73 (F)	493	+	−		Drug (disopyramide), sinus bradycardia
7	30 (F)	502	+	−	KCNH2 (G745fs+55X)*	
8	17 (F)	470	−	−		
9	13 (F)	462	+	−	KCNH2 (a, S320L)	
10	41 (F)	490	−	+		Hypomagnesemia
11	73 (F)	608	+	−	KCNQ1 (a, S277L)	Sinus bradycardia
12	75 (F)	494	+	+		
13	17 (M)	500	−	−		
14	13 (F)	512	+	−		
15	57 (M)	472	−	−		
16	53 (M)	462	+	+		
17	17 (F)	520	+	−		
18	22 (F)	472	−	−		
19	13 (F)	522	−	−	KCNH2 (a, R823W)	
20	13 (M)	467	+	−		
21	52 (M)	524	+	+	KCNH2 (a, R948S)*	Drug (minor tranquilizer), hypokalemia
22	11 (M)	491	−	−		
23	51 (M)	493	−	−		
24	39 (F)	545	−	−		

*Novel variant.
LQTS = long QT syndrome; QTc = corrected QT interval; TdP = torsades de pointes.

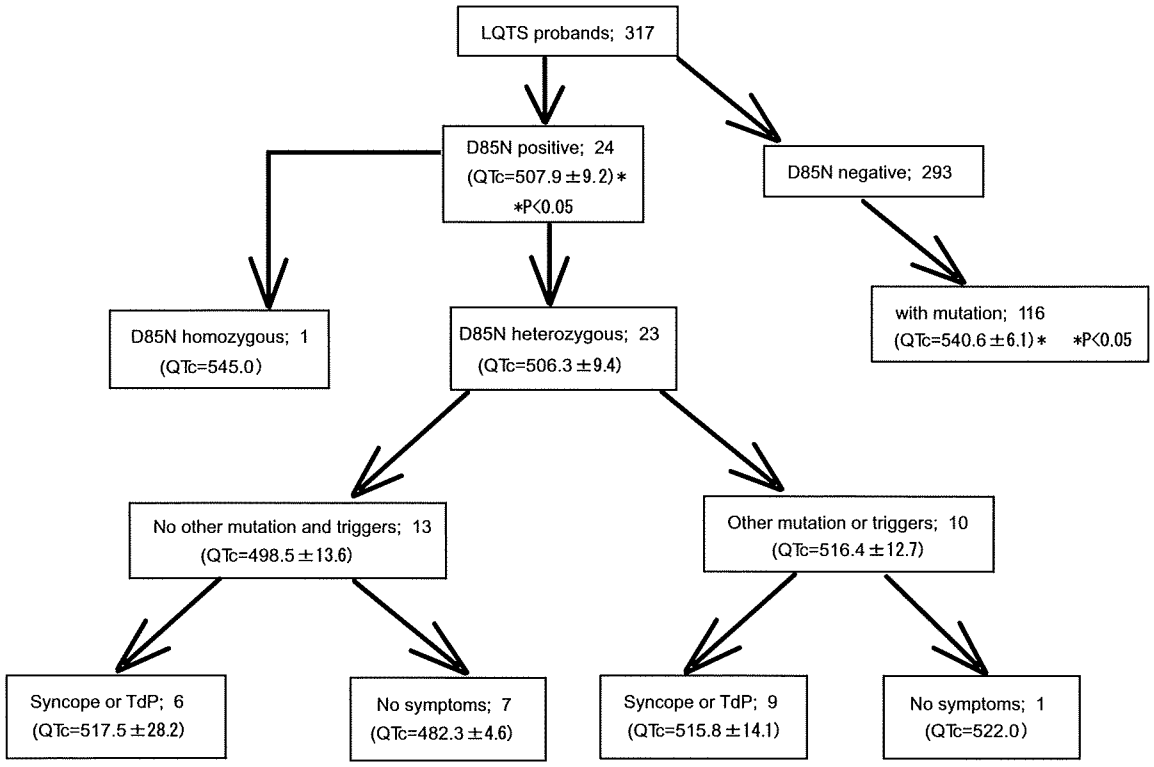

Figure 1 **Summary of LQTS Probands**

LQTS = long QT syndrome; QTc = corrected QT interval; TdP = torsades de pointes.

interval was 35.5 ± 10.4 years. It was significantly older than the mean onset age of the other genotyped symptomatic LQTS patients (21.0 years in our cohort of 94 genotyped LQTS) (Horie M. et al., unpublished data, September 2008). Although the clinical features of KCNE1-D85N–positive probands differed with respect to the QTc and the onset age from those of other genotyped LQTS patients, this variant appeared to be a disease-causing gene variant in congenital LQTS.

Biophysical assays of the genetic variant. **KCNE1-D85N WITH KCNQ1.** In order to confirm that the D85N is a disease-causing variant, we conducted functional assays using a heterologous expression system with a mammalian cell line (CHO cells). In the first line of experiments, we examined how KCNE1-D85N affected the reconstituted KCNQ1/KCNE1 currents. Figure 2 depicts representative current traces recorded from cells that coexpressed KCNQ1 and wild-type (Fig. 2A-a) or D85N (Fig. 2A-b) KCNE1 (1 μg each). Peak tail current densities measured after repolarization to −50 mV from various test pulses were calculated in individual cells and are plotted as a function of test potential in Figure 2B. Solid circles indicate the mean peak current densities from 21 cells that were transfected with KCNQ1 and wild-type KCNE1; open circles indicate the mean peak current densities from 25 cells that were transfected with KCNQ1 and D85N, and solid triangles indicate the mean peak current densities from 25 cells that were transfected with KCNQ1 alone. D85N reduced the peak tail currents of wild-type KCNQ1/KCNE1-encoded currents by 28% at 0 mV test potential ($p < 0.05$ vs. wild type).

In Figure 2C, peak tail current densities have been normalized using the current densities recorded after a test pulse to +50 mV and are plotted as a function of test potential. Fitting of data plots to Boltzmann's equation yielded $V_{0.5}$ values of −4.36 ± 1.8 mV for the wild type and 0.38 ± 1.7 mV for D85N ($p < 0.05$), suggesting that the KCNE1 variant produced a significantly positive shift in KCNQ1-encoded current activation kinetics (Table 2). The deactivation process of tail currents could be fitted by 2 exponentials, yielding fast and slow time constants. No significant difference with respect to the fast time constants was evident between the wild-type and D85N genotypes; however, slow deactivation was significantly accelerated by coexpression of D85N (Table 2).

KCNE1-D85N WITH KCNH2. In the next line of experiments, we examined how KCNE1 and its D85N variant influence KCNH2-encoded currents. Figures 3A-a and 3A-b depict 2 sets of current traces recorded from CHO cells that had been transfected with KCNH2 plus wild-type or D85N KCNE1 (1 μg each). Peak tail current densities at −60 mV were calculated in the respective cells and are plotted as a function of test potential in Figure 3B. Solid circles and open circles indicate the mean current densities calculated from 23

JACC Vol. 54, No. 9, 2009
August 25, 2009:812–9

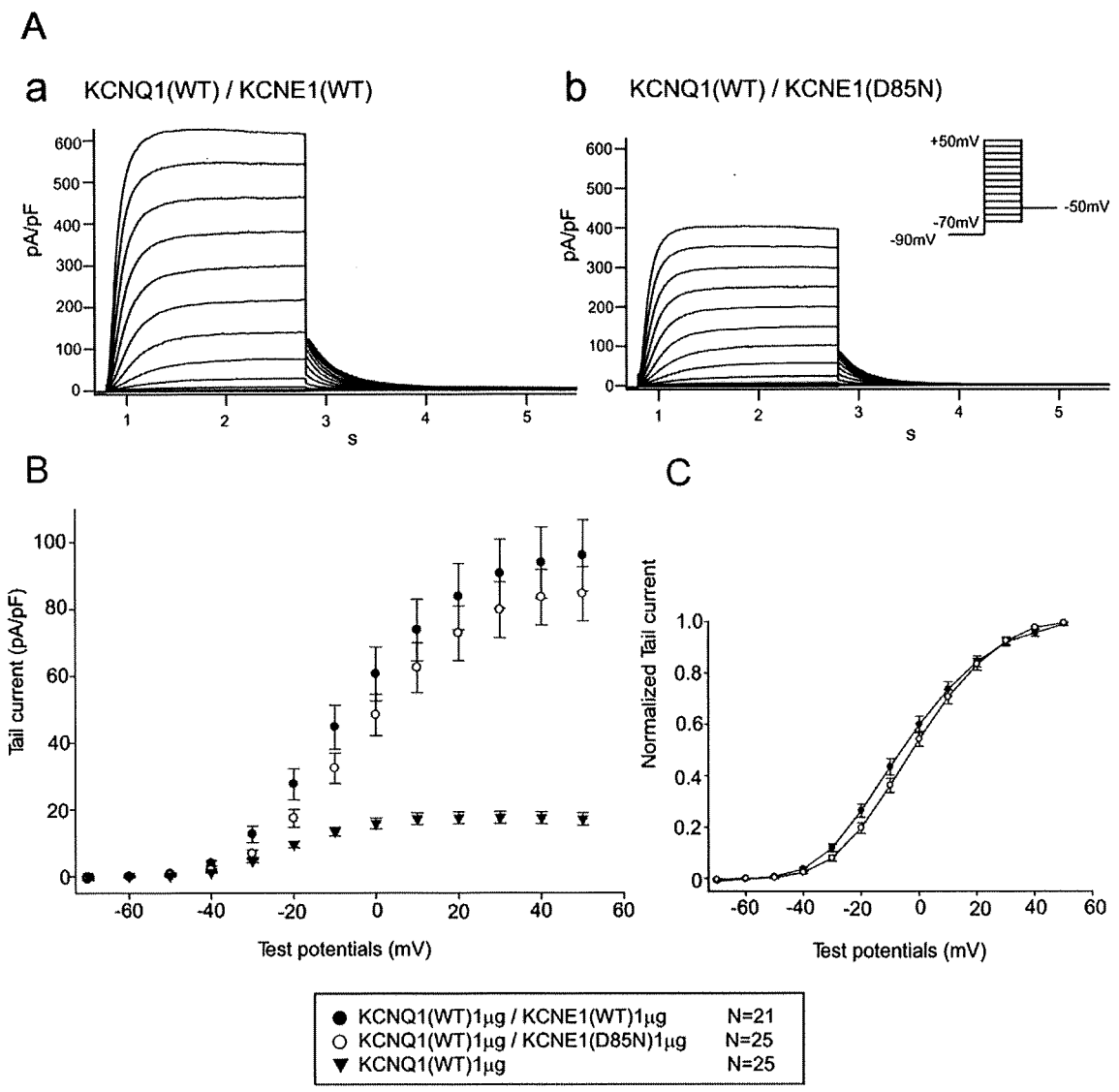

Figure 2 **Functional Expression of KCNQ1 With KCNE1-D85N in Chinese Hamster Ovarian Cells**

(A) Representative current traces of KCNQ1 coexpression with the wild-type (WT) or D85N KCNE1. **(a)** KCNQ1 (1 μg) plus WT KCNE1 (1 μg). **(b)** KCNQ1 (1 μg) plus D85N KCNE1 (1 μg). **(B and C)** Functional consequences of KCNQ1 coexpression with the WT or D85N KCNE1 (**[B]** activation curve; **[C]** normalized activation curve). **Solid circles** indicate the mean peak current densities from 21 cells that have been transfected with KCNQ1 and WT KCNE1 (1 μg of each), and **open circles** indicate the mean peak current densities from 25 cells that have been transfected with KCNQ1 and D85N KCNE1 (1 μg of each). **Solid triangles** show those obtained from 25 cells that were transfected with KCNQ1 alone (1 μg).

and 20 cells, respectively, which were transfected with 1 μg of KCNH2 and 1 μg of wild-type or D85N KCNE1.

D85N reduced the peak tail currents of wild-type KCNH2/KCNE1-encoded currents by 31% to 36% at test potentials between 0 and +50 mV ($p < 0.005$ vs. wild type). Fitting of normalized data to Boltzmann's equation yielded a $V_{0.5}$ of −18.33 ± 0.8 mV for the wild-type KCNH2/KCNE1 and of −22.07 ± 1.6 mV for KCNH2/KCNE1-D85N ($p < 0.05$), suggesting that the KCNE1 variant causes a significantly negative shift of KCNH2/KCNE1-encoded current activation kinetics (Fig. 3C, Table 2). Deactivation of tail currents could be fitted by 2 exponentials, yielding fast and slow time constants. The fast and slow kinetics were not significantly different between the 2 types of KCNH2 channel currents (Table 2).

Discussion

The present study demonstrates that the allele frequency of KCNE1-D85N is significantly higher in LQTS patients than in control subjects after excluding cases with compromised factors to prolong QT interval ($p < 0.05$). A biophysical assay of D85N showed that the variant affected both reconstituted I_{Ks} and I_{Kr} channel function, leading to a prolongation of the QTc with D85N working as a disease-causing variant. In a heterologous expression system with *Xenopus* oocytes (8),

Table 2 $V_{0.5}$, Slope Factor k, and τ Deactivation at +20 mV

	n	$V_{0.5}$	k	τ_{fast}	τ_{slow}
KCNQ1 (WT) 1 μg	25	−20.86 ± 1.034	8.223 ± 0.421	0.070 ± 0.005	0.136 ± 0.019
KCNQ1 (WT) 1 μg/KCNE1 (WT) 1 μg	21	−4.364 ± 1.834*	12.724 ± 0.407*	0.145 ± 0.013*	0.586 ± 0.070†
KCNQ1 (WT) 1 μg/KCNE1 (D85N) 1 μg	25	0.382 ± 1.717*‡	12.566 ± 0.429*	0.141 ± 0.013*	0.409 ± 0.050*‡
KCNH2 (WT) 1 μg/KCNE1 (WT) 1 μg	23	−18.326 ± 0.775	7.373 ± 0.289	0.183 ± 0.016	1.077 ± 0.102
KCNH2 (WT) 1 μg/KCNE1 (D85N) 1 μg	20	−22.069 ± 1.560§	7.037 ± 0.389	0.193 ± 0.013	1.258 ± 0.090

*$p < 0.0001$ versus KCNQ1 (wild type [WT]) 1 μg; †$p = 0.0001$ versus KCNQ1 (WT) 1 μg; ‡$p < 0.05$ versus KCNQ1 (WT) 1 μg/KCNE1 (WT) 1 μg; §$p < 0.05$ versus KCNH2 (WT) 1 μg/KCNE1 (WT) 1 μg.

KCNE1-D85N has been reported to cause an approximately 50% reduction in KCNQ1-encoded currents, although data for mammalian cells is not available. In our experiments using CHO cells, D85N significantly reduced KCNQ1-encoded currents by 28% ($p < 0.05$ vs. wild type), although this effect was smaller than that in *Xenopus* oocytes.

When KCNH2 was coexpressed with the wild-type or D85N variant of KCNE1, D85N significantly reduced wild-type KCNH2/KCNE1-encoded currents by 31% to 36% ($p < 0.005$ vs. wild type). Regarding the interaction between KCNE1 and KCNH2, McDonald et al. (3) demonstrated that KCNE1 forms a stable complex with KCNH2 and

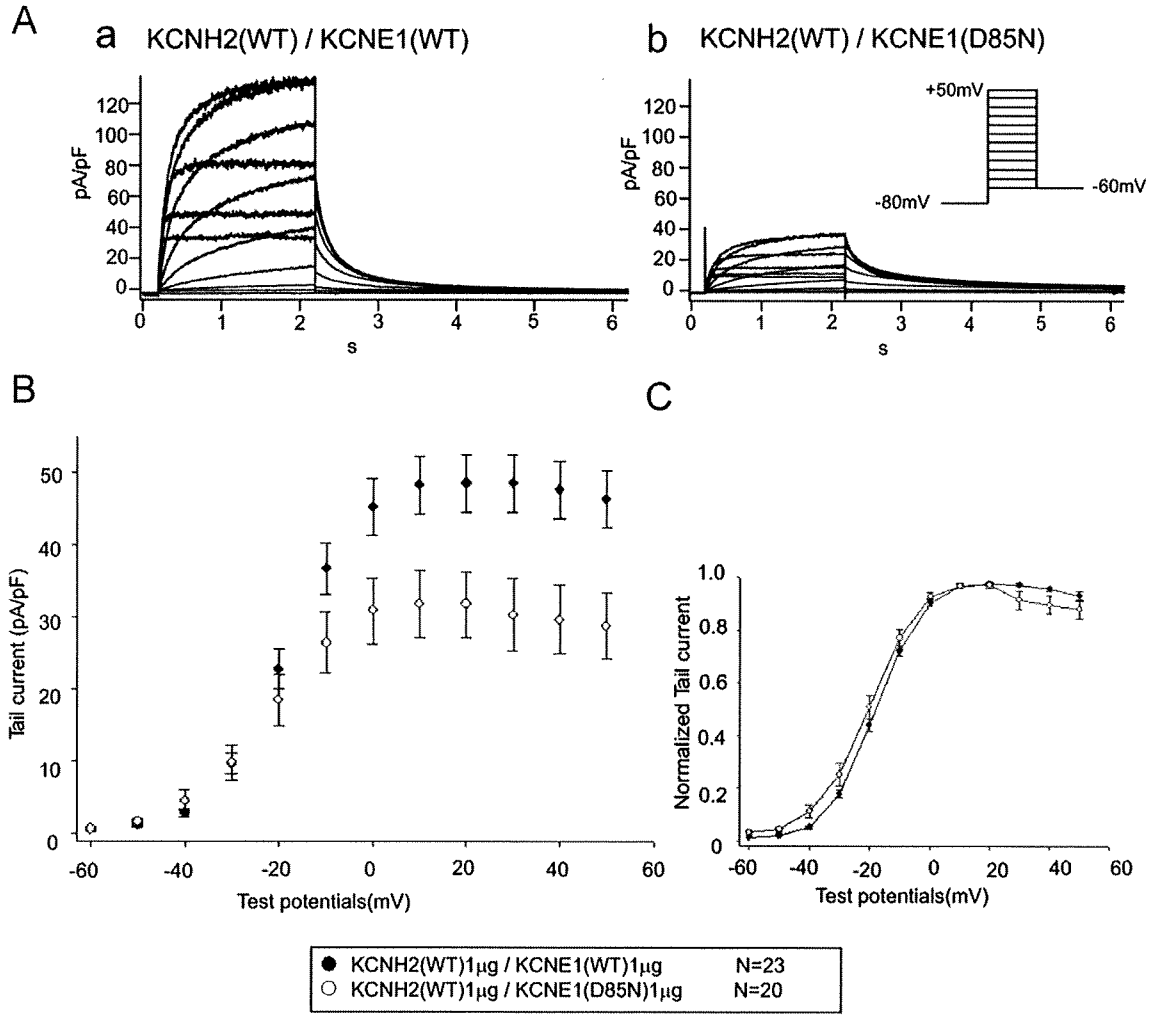

Figure 3 Functional Expression of KCNH2 With KCNE1-D85N in Chinese Hamster Ovarian Cells

(A) Representative current traces of KCNH2 coexpression with the wild-type (WT) or D85N KCNE1. **(a)** KCNH2 (1 μg) plus WT KCNE1 (1 μg). **(b)** KCNH2 (1 μg) plus D85N KCNE1 (1 μg). **(B and C)** Functional consequences of KCNH2 coexpression with the WT or D85N of KCNE1 (**[B]** activation curve; **[C]** normalized activation curve). **Solid circles** indicate data from 23 cells that were transfected with KCNH2 and WT KCNE1 (1 μg of each). **Open circles** indicate data from 20 cells that were transfected with KCNH2 and D85N KCNE1 (1 μg of each).

up-regulates I_{Kr}-like currents by 50% in CHO cells. Bianchi et al. (12) also showed interactions between the KCNE1-D76N mutation and both KCNQ1 and KCNH2 in HEK cells. In atrial tumor myocytes that expressed I_{Kr} alone, Yang et al. (13) demonstrated that antisense oligonucleotides against minK cDNA (KCNE1) significantly reduced the I_{Kr} by ~62%. More recently, Ohno et al. (14) identified a missense KCNE1 mutation, A8V, in a sporadic case of LQTS and reported that the mutation significantly reduced the magnitude of KCNH2- but not KCNQ1-encoded currents.

Collectively, it is of clinical importance that the KCNE1-D85N variant modifies not only KCNQ1- but also KCNH2-coded channel currents. Furthermore, its inhibitory action on KCNH2 was even stronger than that on KCNQ1. The KCNE1-D85N polymorphism may therefore cause phenotypes similar to those observed in type 2 LQTS such as bradycardia (15,16). The deactivation process of I_{Kr} plays a significant role in maintaining the appropriate rate of pacemakers (17) and, therefore, a decreased I_{Kr} will lead to sinus bradycardia. In the present study, 3 D85N carriers (13%) had sinus bradycardia (Table 1).

The mean onset age of 6 symptomatic heterozygous D85N carriers (Table 1) was 35.5 years, and this was significantly older than the mean age of other genotyped symptomatic LQTS patients. Shimizu et al. (18) reported that in 95 Japanese LQT1 patients with transmembrane domain mutations or C-terminal domain mutations, the mean ages of first event were 11 ± 8 years and 13 ± 9 years. Nagaoka et al. (19) also demonstrated that in 118 Japanese LQT2 patients with pore mutations or nonpore mutations, the mean ages of first event were 16 ± 10 years and 20 ± 13 years. In addition, the mean QTc of 13 D85N carriers was prolonged (498.5 ± 13.6 ms) but significantly shorter than that in 116 probands with other LQTS-related gene mutations (541 ms) (Fig. 1). These different phenotypes appear to reflect the fact that D85N causes a milder channel dysfunction than other LQTS mutations, and reveals a "forme fruste" phenotype (20).

The allele frequency of the KCNE1-D85N polymorphism was 0.81% among apparently healthy control individuals. We found only 1 report concerning D85N frequency (0.7%) (7) in control subjects, which showed equivalent results to our study. Based on 2008 healthy French individuals, Gouas et al. (21) demonstrated that the allele frequency of D85N was significantly higher in the 200 subjects with the longest QTc than in those with the shortest QTc (3.1% vs. 0.75%), suggesting that this single nucleotide polymorphism may influence the QTc length in healthy individuals.

LQTS can remain latent or subclinical because of "repolarization reserve" (22), and can become unmasked upon the intake of QT-prolonging drugs. Heterozygous D85N carriers in the control group may be at a potentially higher risk of long QT-related arrhythmias. Assuming that genetic surveys are feasible before drug therapy, D85N carriers may be recommended to avoid the secondary factors that predispose them to further QT prolongation such as QT prolonging drugs (23) and electrolyte disturbances (23–25). It is also clinically useful to search for other variants of long QT-related genes (8,26,27).

Study limitations. In the present study, we screened the mutations that are responsible for LQT1, 2, 3, 5, 6, and 7. Therefore, the comorbidity of other types of LQTS was not completely excluded, although their frequency was quite low. In general, single nucleotide polymorphisms are thought to be nonpathological although some may modify the clinical features of a disease. For example, the KCNH2-K897T polymorphism is a typical genetic modifier that aggravates LQTS phenotypes directly by reducing channel function in association with the KCNH2 mutation A1116V (28). Such a role for KCNE1-D85N was not addressed in this study and warrants further study.

Conclusions

KCNE1-D85N was a highly frequent variant in our LQTS probands and was found to cause loss-of-function effects on both I_{Kr} and I_{Ks} and work as a disease-causing variant. Since its allele frequency was 0.81% among control healthy individuals, KCNE1-D85N may be a clinically important genetic variant.

Acknowledgment

The authors are grateful to the Japanese long QT families for their willingness to participate in this study.

Reprint requests and correspondence: Dr. Minoru Horie, Department of Cardiovascular and Respiratory Medicine, Shiga University of Medical Science, Seta Tsukinowa-cho, Otsu, Shiga 520-2192, Japan. E-mail: horie@belle.shiga-med.ac.jp.

REFERENCES

1. Sanguinetti MC, Curran ME, Zou A, et al. Coassembly of K(V) LQT1 and minK(IsK) proteins to form cardiac I(Ks) potassium channel. Nature 1996;384:80–3.
2. Barhanin J, Lesage F, Guillemare E, Fink M, Lazdunski M, Romey G. K(V)LQT1 and IsK(minK) proteins associate to form the I(Ks) cardiac potassium current. Nature 1996;84:78–80.
3. McDonald TV, Yu Z, Ming Z, et al. A minK-HERG complex regulates the cardiac potassium current $I_{(Kr)}$. Nature 1997;388: 289–92.
4. Sanguinetti MC, Jiang C, Curran ME, Keating MT. A mechanistic link between an inherited and an acquired cardiac arrhythmia: HERG encodes the I_{Kr} potassium channel. Cell 1995;81:299–307.
5. Trudeau MC, Warmke JW, Ganetzky B, Robertson GA. HERG, a human inward rectifier in the voltage-gated potassium channel family. Science 1995;269:92–5.
6. Sanguinetti MC, Curran ME, Spector PS, Keating MT. Spectrum of HERG K^+-channel dysfunction in an inherited cardiac arrhythmia. Proc Natl Acad Sci U S A 1996;93:2208–12.
7. Ackerman MJ, Tester DJ, Jones GS, Will ML, Burrow CR, Curran ME. Ethnic differences in cardiac potassium channel variants: implications for genetic susceptibility to sudden cardiac death and genetic testing for congenital long QT syndrome. Mayo Clin Proc 2003;78: 1479–87.

8. Westenskow P, Splawski I, Timothy KW, Keating MT, Sanguinetti MC. Compound mutations: a common cause of severe long-QT syndrome. Circulation 2004;109:1834–41.
9. Paulussen AD, Gilissen RA, Armstrong M, et al. Genetic variations of KCNQ1, KCNH2, SCN5A, KCNE1, and KCNE2 in drug-induced long QT syndrome patients. J Mol Med 2004;82:182–8.
10. Iwasa H, Itoh T, Nagai R, Nakamura Y, Tanaka T. Twenty single nucleotide polymorphisms (SNPs) and their allelic frequencies in four genes that are responsible for familial long QT syndrome in the Japanese population. J Hum Genet 2000;45:182–3.
11. Keating MT, Sanguinetti MC. Molecular and cellular mechanisms of cardiac arrhythmias. Cell 2001;104:569–80.
12. Bianchi L, Shen Z, Dennis AT, et al. Cellular dysfunction of LQT5-minK mutants: abnormalities of I_{Ks}, I_{Kr} and trafficking in long QT syndrome. Hum Mol Genet 1999;8:1499–507.
13. Yang T, Kupershmidt S, Roden DM. Anti-minK antisense decreases the amplitude of the rapidly activating cardiac delayed rectifier K^+ current. Circ Res 1995;77:1246–53.
14. Ohno S, Zankov DP, Yoshida H, et al. N- and C-terminal KCNE1 mutations cause distinct phenotypes of long QT syndrome. Heart Rhythm 2007;4:332–40.
15. Zhang L, Timothy KW, Vincent GM, et al. Spectrum of ST-T-wave patterns and repolarization parameters in congenital long-QT syndrome: ECG findings identify genotypes. Circulation 2000;102: 2849–55.
16. Nemec J, Buncová M, Bůlková V, et al. Heart rate dependence of the QT interval duration: differences among congenital long QT syndrome subtypes. J Cardiovasc Electrophysiol 2004;15:550–6.
17. Ono K, Ito H. Role of rapidly activating delayed rectifier K+ current in sinoatrial node pacemaker activity. Am J Physiol 1995; 269:H453–62.
18. Shimizu W, Horie M, Ohno S, et al. Mutation site-specific differences in arrhythmic risk and sensitivity to sympathetic stimulation in the LQT1 form of congenital long QT syndrome: multicenter study in Japan. J Am Coll Cardiol 2004;44:117–25.
19. Nagaoka I, Shimizu W, Itoh H, et al. Mutation site dependent variability of cardiac events in Japanese LQT2 form of congenital long-QT syndrome. Cir J 2008;72:694–9.
20. Priori SG, Napolitano C, Schwartz PJ. Low penetrance in the long QT syndrome. Clinical impact. Circulation 1999;99:529–33.
21. Gouas L, Nicaud V, Berthet M, et al. Association of KCNQ1, KCNE1, KCNH2 and SCN5A polymorphisms with QTc interval length in a healthy population. Eur J Hum Genet 2005;13:1213–22.
22. Xiao L, Xiao J, Luo X, Lin H, Wang Z, Nattel S. Feedback remodeling of cardiac potassium current expression: a novel potential mechanism for control of repolarization reserve. Circulation 2008;118: 983–92.
23. Roden DM, Viswanathan PC. Genetics of acquired long QT syndrome. J Clin Invest 2005;115:2025–32.
24. Justo D, Prokhorov V, Heller K, Zeltser D. Torsade de pointes induced by psychotropic drugs and the prevalence of its risk factors. Acta Psychiatr Scand 2005;111:171–6.
25. Kusano KF, Hata Y, Yumoto A, Emori T, Sato T, Ohe T. Torsade de pointes with a normal QT interval associated with hypokalemia: a case report. Jpn Circ J 2001;65:757–60.
26. Schwartz PJ, Priori SG, Napolitano C. How really rare are rare diseases?: the intriguing case of independent compound mutations in the long QT syndrome. J Cardiovasc Electrophysiol 2003;14:1120–1.
27. Hsieh MH, Chen SA, Chiang CE, et al. Drug-induced torsades de pointes in one patient with congenital long QT syndrome. Int J Cardiol 1996;54:85–8.
28. Crotti L, Lundquist AL, Insolia R, et al. KCNH2-K897T is a genetic modifier of latent congenital long-QT syndrome. Circulation 2005; 112:1251–8.

Key Words: long QT syndrome ■ single nucleotide polymorphism ■ disease-causing variant.

THE JOURNAL OF BIOLOGICAL CHEMISTRY VOL. 284, NO. 32, pp. 21580–21588, August 7, 2009

Tuberous Sclerosis Tumor Suppressor Complex-like Complexes Act as GTPase-activating Proteins for Ral GTPases*[S]

Received for publication, April 24, 2009, and in revised form, June 10, 2009 Published, JBC Papers in Press, June 11, 2009, DOI 10.1074/jbc.M109.012112

Ryutaro Shirakawa[‡1], Shuya Fukai[§], Mitsunori Kawato[‡2], Tomohito Higashi[‡1,3], Hirokazu Kondo[‡4], Tomoyuki Ikeda[‡], Ei Nakayama[‡], Katsuya Okawa[¶], Osamu Nureki[‖], Takeshi Kimura[‡], Toru Kita[‡5], and Hisanori Horiuchi[‡6]

From the [‡]Department of Cardiovascular Medicine and [¶]Frontier Technology Center, Graduate School of Medicine, Kyoto University, Kyoto 606-8507, Japan, the [§]Structural Biology Laboratory, Life Science Division, Synchrotron Radiation Research Organization and Institute of Molecular and Cellular Biosciences, The University of Tokyo, Tokyo 113-0032, Japan, and the [‖]Department of Basic Medical Sciences, The Institute of Medical Science, The University of Tokyo, Tokyo 108-8639, Japan

The small GTPases RalA and RalB are multifunctional proteins regulating a variety of cellular processes. Like other GTPases, the activity of Ral is regulated by the opposing effects of guanine nucleotide exchange factors (GEFs) and GTPase-activating proteins (GAPs). Although several RalGEFs have been identified and characterized, the molecular identity of RalGAP remains unknown. Here, we report the first molecular identification of RalGAPs, which we have named RalGAP1 and RalGAP2. They are large heterodimeric complexes, each consisting of a catalytic α1 or α2 subunit and a common β subunit. These RalGAP complexes share structural and catalytic similarities with the tuberous sclerosis tumor suppressor complex, which acts as a GAP for Rheb. *In vitro* GTPase assays revealed that recombinant RalGAP1 accelerates the GTP hydrolysis rate of RalA by 280,000-fold. Heterodimerization was required for this GAP activity. In PC12 cells, knockdown of the β subunit led to sustained Ral activation upon epidermal growth factor stimulation, indicating that the RalGAPs identified here are critical for efficient termination of Ral activation induced by extracellular stimuli. Our identification of RalGAPs will enable further understanding of Ral signaling in many biological and pathological processes.

Members of the Ras superfamily of small GTPases act as molecular switches by cycling between an inactive GDP-bound conformation and an active GTP-bound conformation. In their GTP-bound form, small GTPases interact with their effector proteins to induce downstream signaling events. The GDP/GTP cycling is strictly regulated by two classes of regulatory proteins termed guanine nucleotide exchange factors (GEFs)[7] and GTPase-activating proteins (GAPs) (1). GEFs activate GTPases by inducing the release of bound GDP for subsequent GTP binding. GAPs inactivate GTPases by accelerating the slow intrinsic rate of GTP hydrolysis.

The Ras-like small GTPases, RalA and RalB, regulate a large variety of cellular processes including transcription, translation, cytoskeletal organization, membrane trafficking, cytokinesis, cell migration, cell proliferation, and cell survival (for review, see Ref. 2–4). RalA and RalB are highly similar to each other (81% amino acid identity) and share the same effectors, such as the exocyst complex (5–7) and RalBP1/RLIP76 (8, 9). Despite this similarity, functional differences between the two isoforms have been described; RalA is indispensable for the anchorage-independent proliferation of tumor cells (10–13), whereas RalB counters apoptotic signaling to support survival of tumor cells (10, 14). To date, six RalGEF proteins have been identified and characterized. They are structurally classified into two major groups. Members of the RalGDS family, which includes RalGDS (15), Rgl (16), Rlf (17), and Rgl3 (18), possess a Ras binding domain and are directly activated by binding to Ras-GTP (19, 20). Another class of RalGEFs consists of RalGPS1/RalGEF2 (21, 22) and RalGPS2 (21, 23). This novel type of RalGEF lacks the Ras binding domain but, instead, has a pleckstrin homology domain.

The finding that Ras can activate most RalGEFs in addition to Raf and phosphoinositide 3-kinases suggested that Ral GTPases mediate some functions of oncogenic Ras. Recent studies using human cells have revealed an essential contribution of this Ras-RalGEFs-Ral signaling pathway to Ras-induced tumorigenic transformation (24, 25). Although these studies highlight the importance of appropriate regulation of Ral activity in normal cells, the negative regulators for Ral GTPases, namely RalGAPs, have not yet been identified. A report by Feig and co-workers (26) demonstrated the

* This work was supported by Research Grants 15081206 and 20013201 (to H. H.) and 07J08426 (to R. S.) from the Ministry of Education, Culture, Sports, Science, and Technology of Japan and the Takeda Science Foundation (to H. H.) This work was also supported in part by Global COE Program "Center for Frontier Medicine" from the Ministry of Education, Culture, Sports, Science, and Technology.

[S] The on-line version of this article (available at http://www.jbc.org) contains supplemental Figs. 1 and 2.

The nucleotide sequence reported in this paper has been submitted to the DDBJ/GenBank™/EBI Data Bank with accession numbers AB511280.

[1] Supported by the Japan Society for the Promotion of Science Research Fellowship for Young Scientists.

[2] Present address: Nishi-Kobe Medical Center, Kobe 651-2273, Japan.

[3] Present address: Division of Cell Biology, Graduate School of Medicine, Kobe University, Kobe 650-0017, Japan.

[4] Present address: Osaka Red Cross Hospital, Osaka 543-8555, Japan.

[5] Present address: Kobe City Medical Center General Hospital, Kobe 650-0046, Japan.

[6] To whom correspondence should be addressed. Dept. of Cardiovascular Medicine, Graduate School of Medicine, Kyoto University, Kyoto 606-8507, Japan. Tel.: 81-75-751-3195; Fax: 81-75-751-3203; E-mail: horiuchi@kuhp.kyoto-u.ac.jp.

[7] The abbreviations used are: GEF, guanine nucleotide exchange factor; GAP, GTPase-activating protein; GST, glutathione *S*-transferase; GppNHp, guanosine 5′-(β,γ-imido)triphosphate; EGF, epidermal growth factor; ERK, extracellular signal-regulated kinase; siRNA, short interfering RNA.

existence of Ral-specific GAP activity in the cytosolic fraction of brain and testis. However, the molecule(s) responsible for this GAP activity still remains elusive.

In this study we report the molecular identification of RalGAPs, which we have named RalGAP1 and RalGAP2. They are large heterodimeric complexes, each composed of a catalytic $\alpha 1$ or $\alpha 2$ subunit and a common β subunit. Interestingly, the RalGAP complexes have structural and catalytic similarities to the tuberous sclerosis tumor suppressor complex.

EXPERIMENTAL PROCEDURES

Purification of the p240-p170 Complex from Porcine Brain Cytosol—All purification procedures were performed at 4 °C unless otherwise noted. Eight porcine brains were homogenized in 1.6 liters of buffer A (50 mM HEPES/KOH, pH 7.4, 78 mM KCl, 4 mM $MgCl_2$, 2 mM EGTA, 0.2 mM $CaCl_2$, 1 mM dithiothreitol) containing protease inhibitors (protease inhibitor mixture for mammalian cells; Sigma) using a Waring blender followed by a glass-Teflon homogenizer. The homogenate was centrifuged at 2800 × *g* for 30 min to remove coarse particulates. The supernatant was dialyzed overnight against 5 liters of buffer A. The dialyzed material was further centrifuged at 120,000 × *g* for 1 h to obtain clarified cytosol (~5 mg of protein ml^{-1}, 1.2 liters). The cytosol was supplemented with the nonhydrolyzable GTP analogue guanosine 5′-(β,γ-imido)triphosphate (GppNHp) (10 μM; Sigma) and used for $RalA^{Q72L}$ affinity chromatography as described below.

For preparation of the affinity column, glutathione *S*-transferase (GST)-$RalA^{Q72L}$ (residues 9–183, 160 mg) was immobilized on 8 ml of glutathione beads (Glutathione-Sepharose 4B; GE Healthcare). $RalA^{Q72L}$-bound nucleotides were exchanged for GppNHp by incubating the beads in buffer A containing 10 mM EDTA and 1 mM GppNHp at room temperature for 90 min. The GppNHp-bound form of $RalA^{Q72L}$ was stabilized by adding $MgCl_2$ to a final concentration of 14 mM. These affinity beads were packed into the PolyPrep columns (Bio-Rad), and porcine brain cytosol prepared as above was loaded onto these columns. After washing the columns with 20 column volumes of buffer A, bound proteins were eluted with 2 column volumes of buffer B (50 mM HEPES, KOH, pH 7.4, 78 mM KCl, 10 mM EDTA, 1 mM dithiothreitol, 5 mM GDP). The eluate (16 ml) was passed through a glutathione beads column (0.4 ml) to remove GST-$RalA^{Q72L}$ that leaked from the affinity column during the elution step and then concentrated to ~0.6-ml using a Centriprep YM-100 (Millipore). The concentrated sample was applied to a Superose 6 10/300 GL gel filtration column (GE Healthcare) equilibrated with buffer A, and fractions of 0.6 ml were collected. Fractions were analyzed by SDS-PAGE and Coomassie Blue staining. Protein bands of p240 and p170 were excised from the gel and subjected to mass spectrometry analyses as described previously (27, 28).

Purification of the p220-p170 Complex from Rat Lung Cytosol—We performed essentially the same purification scheme used for the p240-p170 complex purification except that purification was performed on a 1/10 scale with freshly isolated lungs of thirty male Wister rats. The affinity column eluate was fractionated on a Superose 6 PC3.2/30 column (SMART chromatography system; GE Healthcare), and fractions containing p170 (fractions 17–22) were pooled and used for GTPase assays. As a comparison, we treated rat brains in the same fashion.

Plasmid Constructs and Recombinant Proteins—We amplified full-length p240 cDNA by PCR from human brain Marathon-Ready cDNA (BD Biosciences) and cloned it into the XhoI site of pBluescript II SK(+) (Stratagene). We sequenced six independent clones and found that all of them contained a 141-bp insertion after bp 2266 of the deposited cDNA sequence for *Homo sapiens* GTPase-activating Rap/Ran GAP domain-like 1 (NM_014990). This insertion encodes a 47-amino acid sequence without changing the reading frame. The N1950K mutation was introduced by PCR-based site-directed mutagenesis. The p170 cDNA (KIAA1219) was obtained from Kazusa DNA Research Institute (Chiba, Japan). These cDNAs were subcloned into pFastBac HT to generate recombinant baculoviruses (Bac-to-Bac Baculovirus Expression System; Invitrogen). The cDNAs for RalA, RalB, H-Ras, Rap1A, Rheb, RhoA (27), Rab27A, Ran, Sec5 Ral binding domain (residues 1–120) (28), and Raf1 Ras binding domain (residues 51–131) were amplified by PCR from human brain or bone marrow Marathon-Ready cDNA and cloned into pGEX-2T (GE Healthcare). The truncated version of RalA (residues 9–183) (29) with a Q72L mutation was generated by PCR and subcloned into pGEX-2T. All constructs were verified by DNA sequencing.

His_6-tagged p240 and p170 were expressed in Sf9 insect cells and affinity-purified on nickel beads (nickel-nitrilotriacetic acid-agarose; Qiagen). Purified proteins were concentrated and further purified on a Superose 6 PC3.2/30 gel filtration column equilibrated with buffer A. The peak fractions were stored at 4 °C and used for GTPase assays within 3 days. GST fusion proteins were expressed in *Escherichia coli* strain BL21 (DE3) transformed with the corresponding pGEX plasmids and affinity-purified on glutathione beads. Purified proteins were dialyzed against buffer A, snap-frozen in liquid nitrogen, and stored at −80 °C until use. Protein concentrations were determined by the Bradford assay (Bio-Rad) or by densitometry of Coomassie Blue-stained gels using bovine serum albumin as a standard in both cases.

GTPase Assays—We assessed GAP activity using a nitrocellulose filter binding assay or thin layer chromatography. For the filter binding assay, GST fusion GTPases were loaded with [γ-^{32}P]GTP in buffer A containing 10 mM EDTA and 10 μM [γ-^{32}P]GTP (~3000 cpm $pmol^{-1}$; PerkinElmer Life Sciences) at 30 °C for 15 min. Loading reactions were stopped by chilling on ice and adding $MgCl_2$ to a final concentration of 14 mM. GTPase assays were performed at 30 °C in 20-μl mixtures containing 20 pmol of labeled GTPases and test materials. Reactions were stopped by diluting the 20-μl mixtures into 0.8 ml of ice-cold buffer A and filtering on 0.45-μm nitrocellulose filters (Whatman). Filters were washed twice with 4 ml of ice-cold buffer A, dried, and counted in a liquid scintillation counter. For the thin layer chromatography analysis, GTPase assays were performed with GST fusion GTPases preloaded with [α-^{32}P]GTP (~6000 cpm $pmol^{-1}$; PerkinElmer). Nucleotides trapped on the filters were eluted at 85 °C for 3 min with buffer A containing 0.1% SDS, 10 mM EDTA, 1 mM GTP, and 1 mM GDP. Released nucleotides were spotted on polyethyleneimine cellulose plates (Merck) and chromatographed with 1 M LiCl

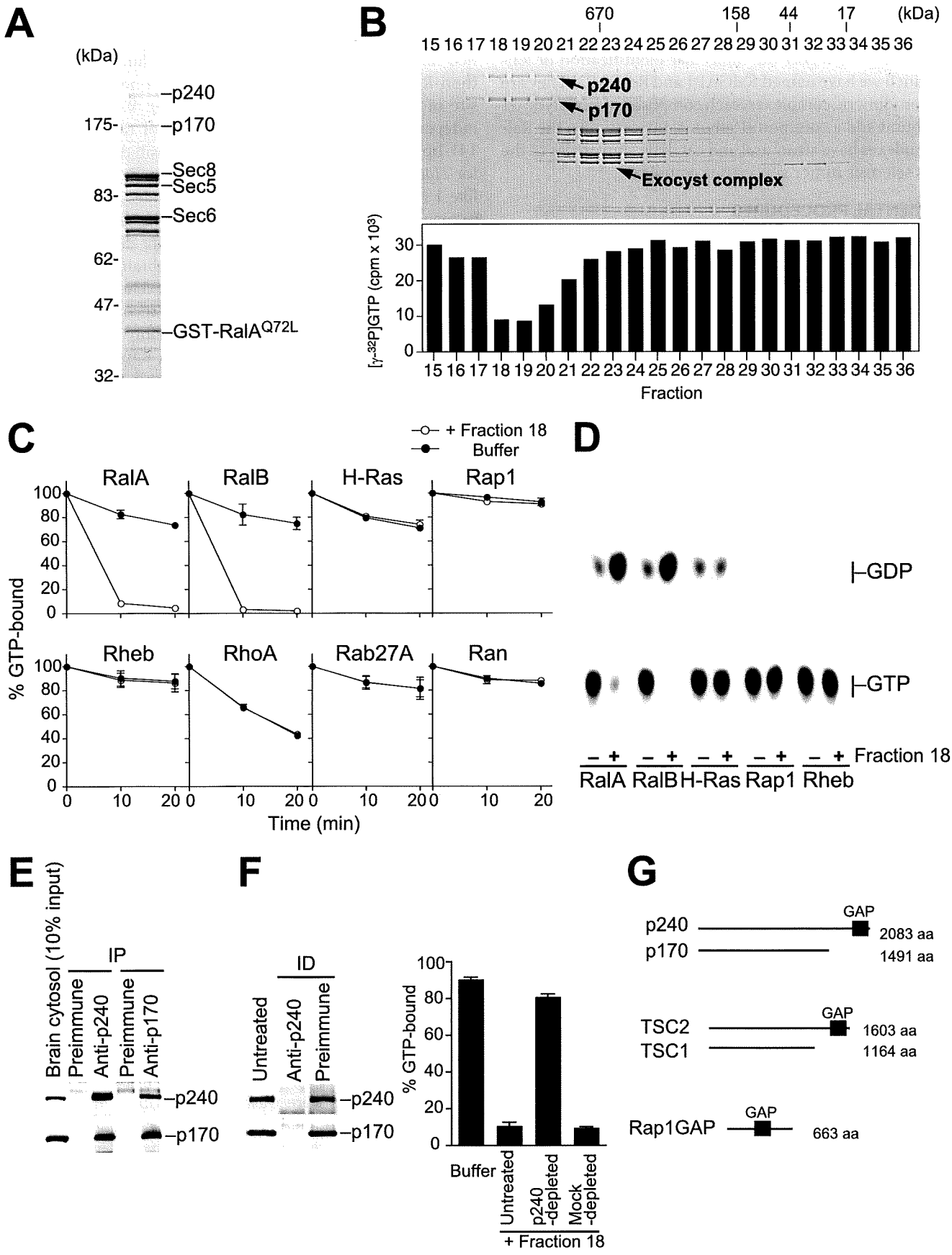

and 1 M formic acid. Plates were dried and processed for autoradiography.

Antibodies—Rabbit anti-p240 polyclonal antibodies were raised against a recombinant fragment of p240 (residues 803–1080) and the following synthetic peptides: MFSKKPHGDVKKSTQKVLD (residues 1–19) and SMSDQEKPEEPPTSNEC (residues 1630–1646). We used the anti-recombinant p240 antibody for Western blot analysis and the anti-peptide antibodies for immunoprecipitation assays. Rabbit anti-p170 antibody was raised against the peptide KRLESDSYSPPHVRRKQKI (residues 1442–1460). Rabbit anti-p220 antibody was raised against the peptide AQEDADKLGLSETDSKE (residues 451–467). Other antibodies used were anti-RalA, -Ras, -Sec6, -Sec8, (BD Biosciences), anti-tubulin α (Sigma), anti-phospho-extracellular signal-regulated kinase (ERK) 1/2 (Santa Cruz Biotechnology), anti-Sec5 (28), and horseradish peroxidase-labeled anti-rabbit or -mouse IgG (GE Healthcare).

Immunoprecipitation and Immunodepletion Assays—For immunoprecipitation assays, porcine brain cytosol (Fig. 1*E*), rat testis cytosol (Fig. 3*B*), or rat lung cytosol (Fig. 3*E*) were incubated at 4 °C for 3 h with the indicated antibodies prebound to protein A beads (Protein A-agarose; Roche Applied Science). Where indicated, immunoprecipitates were prepared in the presence of 50 μg of antigen peptides. Beads were washed 4 times with buffer A containing 0.1% (w/v) Triton X-100, and proteins bound to the beads were analyzed by Western blotting. In Fig. 3*E*, washed beads were directly incubated with radiolabeled GTPases. For immunodepletion assays, 10 μl of packed protein A beads were incubated at 4 °C for 1 h with the indicated antisera (20 μl each) and then washed 5 times with buffer A. Aliquots of fraction 18 (Fig. 1*F*) or the pooled lung fraction (Fig. 3*C*) were incubated with the IgG-coated beads at 4 °C for 3 h. Beads were removed by brief centrifugation, and the supernatants were used for GTPase assays.

Tissue Distribution Analysis—Various organs from male Wister rats were homogenized in buffer A containing protease inhibitors. The homogenates were centrifuged at 2,000 × *g* for 10 min, and the supernatants were further centrifuged at 200,000 × *g* for 10 min. Aliquots of the resulting supernatants (100 μg total protein) were analyzed by Western blotting with the indicated antibodies.

Knockdown and Pulldown Assays—We used two distinct short interfering RNAs (siRNAs) targeting rat/mouse p170 (Stealth™ RNAi; Invitrogen): 5′-GAAACCUGGGAAGUCUUACUGUUGU-3′ (p170 siRNA#1) and 5′-GAUUGAUGUUGUGGUUCCUUACUUU-3′ (p170 siRNA#2). Their scrambled sequences were used as controls. PC12 cells were maintained in Dulbecco's modified Eagle's medium supplemented with 10% fetal bovine serum and 10% horse serum in 6-cm culture dishes. Cells at ~40% confluency were transfected with the individual siRNAs (50 nM) with RNAiMAX transfection regent (Invitrogen). Seventy-two hours after transfection cells were rinsed once with phosphate-buffered saline and lysed in 0.8 ml of ice-cold buffer C (50 mM HEPES/KOH, pH 7.4, 100 mM NaCl, 4 mM $MgCl_2$, 2 mM EGTA, 1 mM dithiothreitol, 1% (w/v) Triton X-100, 10 mM β-glycerophosphate, 10 mM NaF, 1 mM Na_3VO_4) containing protease inhibitors. Lysates were rotated at 4 °C for 5 min and then centrifuged at 200,000 × *g* for 5 min. The supernatants were incubated at 4 °C for 30 min with glutathione beads precoated with 20 μg of GST-Sec5 Ral binding domain. After washing the beads three times with buffer C, bead-associated RalA was analyzed by Western blotting. Part of the supernatants was taken before the incubation and used for Western blot analysis to assess knockdown efficiencies. NIH3T3 cells were lysed at 48 h after siRNA transfection and processed as described above. For epidermal growth factor (EGF) stimulation assays, we used the p170 siRNA#1 and siRNA#2 in combination at 25 nM each. PC12 cells treated with the siRNAs were serum-starved for 8 h and then stimulated with EGF (20 ng ml^{-1}; R&D Systems). After stimulation, cells were harvested in buffer C at the indicated time points, and the GTP-bound forms of RalA and Ras were pulled down using glutathione beads precoated with both GST-Sec5 Ral binding domain and GST-Raf1 Ras binding domain (20 μg each).

RESULTS AND DISCUSSION

Affinity Purification of RalGAP Complex from Porcine Brain Cytosol—To purify RalGAP, we applied an affinity chromatography approach using $RalA^{Q72L}$ as bait. In general, Ras family GTPases with a glutamine to leucine substitution in the switch II region (Q61L in Ras) are resistant to GAP-stimulated GTP hydrolysis, whereas these mutants can still bind to their cognate GAPs (1). Ras^{Q61L}, although unable to hydrolyze GTP efficiently, has higher affinities than wild type for RasGAPs, $p120^{GAP}$, and NF1/neurofibromin (22, 23). Therefore, we reasoned that the analogous mutant $RalA^{Q72L}$ would be ideal bait for RalGAP. We prepared an affinity column immobilized with GST-$RalA^{Q72L}$ preloaded with GppNHp, a non-hydrolyzable GTP analogue, and searched for binding proteins in porcine brain cytosol.

We observed 14 proteins eluting from the column with EDTA and GDP (Fig. 1*A*). Among them, we identified components of the exocyst complex, a known effector of Ral GTPases (5–7), thus confirming the specificity of the affinity purification. We then separated the mixture of $RalA^{Q72L}$-binding pro-

FIGURE 1. **The p240-p170 complex purified from porcine brain has RalGAP activity.** *A*, $RalA^{Q72L}$ affinity column eluate was analyzed by SDS-PAGE and Coomassie Blue staining. Components of the exocyst complex (Sec8, Sec5, and Sec6) and GST-$RalA^{Q72L}$ that had leaked from the column are indicated, as identified by Western blotting (not shown). *B*, *upper panel*, the mixture of $RalA^{Q72L}$-binding proteins was separated on a Superose 6 gel filtration column, and the resulting fractions were analyzed by SDS-PAGE and Coomassie blue staining. *Lower panel*, each fraction was tested for RalGAP activity by a filter binding assay using [γ-^{32}P]GTP-loaded RalA as described under "Experimental Procedures." *C*, various Ras family GTPases preloaded with [γ-^{32}P]GTP were incubated at 30 °C for the indicated periods with (*open circles*) or without (*closed circles*) fraction 18, and the [γ-^{32}P]GTP remaining bound to GTPases was measured by the filter binding assay (mean ± S.E., $n = 2$). *D*, Ras subfamily GTPases preloaded with [α-^{32}P]GTP were incubated at 30 °C for 10 min with (+) or without (−) fraction 18, and bound nucleotides were analyzed by thin layer chromatography and autoradiography. *E*, co-immunoprecipitation of p240 and p170 from porcine brain cytosol. *IP*, immunoprecipitation. *F*, immunodepletion of p240 from fraction 18 results in a concomitant depletion of p170 (*left panel*) and abolishes the GAP activity for RalA (*right graph*) (mean ± S.E., $n = 3$). *ID*, immunodepletion. *G*, schematic comparison of the domain structure of the p240-p170 complex, the TSC2-TSC1 complex, and Rap1GAP. *aa*, amino acids.

Identification of RalGAPs

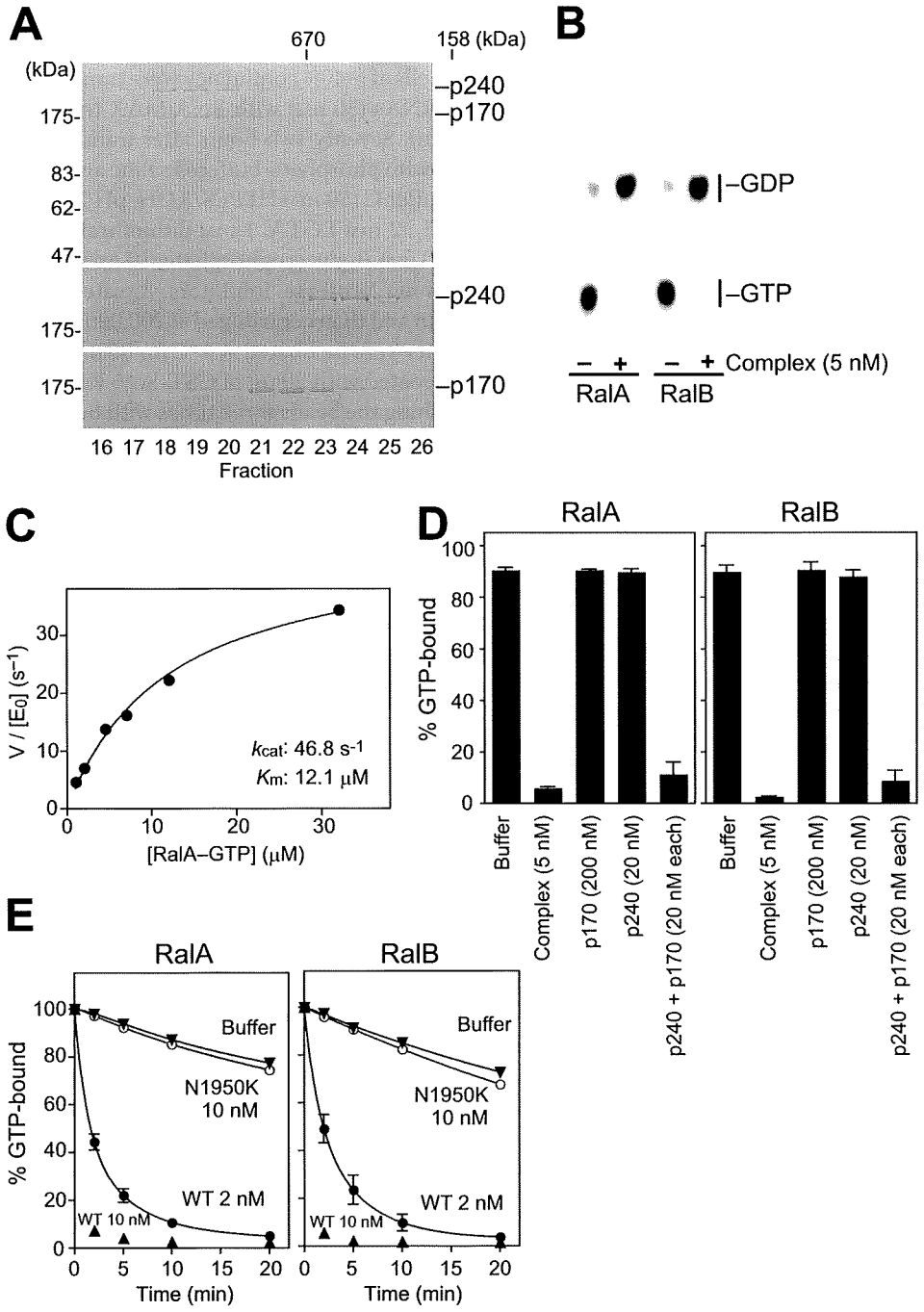

FIGURE 2. **Biochemical and catalytic properties of the recombinant p240-p170 complex.** *A*, chromatographic comparison of the recombinant p240-p170 complex (*top*), p240 alone (*middle*), and p170 alone (*bottom*) on Superose 6 gel filtration chromatography. Gels were Coomassie Blue-stained. *B*, autoradiograph showing that the recombinant complex stimulates Ral GTPase activity. [α-^{32}P]GTP-loaded RalA or RalB were incubated at 30 °C for 10 min with (+) or without (−) the recombinant complex (5 nM). *C*, kinetic analysis of the recombinant p240-p170 complex. Initial rates of GTP hydrolysis on RalA were determined at 30 °C at increasing concentrations of GTP-bound RalA by the filter binding assay. The recombinant p240-p170 complex was used at 1 nM ($[E_o]$). GTPase reaction rates were fitted to the Michaelis-Menten equation to give K_m (12.1 μM) and k_{cat} (46.8 s^{-1}) values of the reaction. *D*, p240 requires p170 for GAP activity. [γ-^{32}P]GTP-loaded RalA or RalB were incubated at 30 °C for 10 min with the recombinant complex, p240 alone, p170 alone, or a mixture of separately purified p240 and p170 at the indicated concentrations (mean ± S.E., $n = 3$). *E*, the N1950K mutation abrogates p240 GAP activity. [γ-^{32}P]GTP-loaded RalA or RalB were incubated at 30 °C for the indicated periods with the wild-type complex (*WT*; 2 nM or 10 nM) or the mutant complex (*N1950K*; 10 nM) (mean ± S.E., $n = 3$).

teins by gel filtration chromatography and tested the fractions for RalGAP activity. Activity was monitored by incubating each fraction with [γ-^{32}P]GTP-loaded RalA and measuring the decrease in radioactivity that remained bound to RalA. We detected a marked activity in fractions with an apparent molecular mass of >1000 kDa (Fig. 1*B*, fractions 18–20). Interestingly, proteins of 240 kDa (p240) and 170 kDa (p170) both co-fractionated with this activity (Fig. 1*B*, *upper panel*). As clearly seen in Fig. 1*C*, the activity in fraction 18 was highly specific for RalA and RalB among the Ras family GTPases tested. Moreover, the activity was indeed due to acceleration of GTP hydrolysis, but not to GTP dissociation, because [α-^{32}P]GTP bound to RalA or RalB was specifically hydrolyzed to GDP after incubation with fraction 18, as analyzed by thin layer chromatography (Fig. 1*D*). These results indicated that fraction 18, which contained only p240 and p170, had GAP activity toward Ral GTPases.

Molecular Identification of p240 and p170—Mass spectrometry analysis revealed p240 to be the porcine orthologue of human GTPase-activating Rap/RanGAP domain-like 1 (GARNL1, also known as tuberin-like protein 1 or KIAA0884), the gene for which was identified as a candidate for 14q13-linked neurological disorders (32). p170 was identified to be the porcine orthologue of human KIAA1219, an evolutionarily conserved protein of unknown function. We generated polyclonal antibodies against the two proteins and confirmed these results (data not shown).

Because p240 and p170 co-migrated in the gel filtration (Fig. 1*B*), we tested whether the two proteins formed a complex. As shown in Fig. 1*E*, p240 and p170 were co-immunoprecipitated from porcine brain crude cytosol with either the anti-p240 or anti-p170 antibodies. Immunodepletion of p240 from fraction 18 with anti-p240 IgG-coated beads resulted in a concomitant depletion of p170 (Fig. 1*F*, *left*) and abolished the activity in the fraction (Fig. 1*F*, *right*). Thus, p240 and p170 form a stoichiometric complex that acts as RalGAP.

The C-terminal ~200-amino acid region of p240 shows a high degree of sequence identity to the catalytic domain of TSC2/tuberin (31% amino acid identity) and to a lesser extent

that of Rap1GAP (24% identity) (supplemental Fig. 1*A*). Apart from this region, p240 has no other discernible domains. TSC2 is a tumor suppressor protein that acts as a GAP toward Rheb (33–37), a Ras subfamily GTPase that promotes cell growth through activation of the mTOR pathway. TSC2 functions in a complex with a non-catalytic subunit TSC1/hamartin. Loss of either TSC2 or TSC1 leads to constitutive activation of Rheb and causes the benign tumor syndrome tuberous sclerosis (38). Notably, the p240-p170 complex has a similar domain organization as the TSC2-TSC1 complex (Fig. 1*G*), although there is no sequence similarity between p170 and TSC1.

Biochemical and Catalytic Properties of the Recombinant p240-p170 Complex—Next, we characterized the biochemical and catalytic properties of the complex using His_6-tagged recombinant forms of human p240 and p170. We could purify the proteins at a nearly stoichiometric ratio from Sf9 insect cells co-infected with baculoviruses encoding each protein. Gel filtration analysis showed that the purified proteins eluted together at >1000 kDa (Fig. 2*A*, *top*), which is similar to the elution properties of the brain native complex (Fig. 1*B*). In contrast, p240 alone or p170 alone, which were purified from separately infected cells, eluted around 450 or 700 kDa, respectively (Fig. 2*A*, *middle* and *bottom*). This observation again indicates that the two proteins interact directly to form a stable complex. The recombinant complex exhibited potent GAP activity toward RalA and RalB (Fig. 2*B*). Kinetic analysis revealed that the complex acts on RalA with K_m and k_{cat} values of 12.1 μM and 46.8 s^{-1}, respectively (Fig. 2*C*). Because the intrinsic GTP hydrolysis rate of RalA is calculated to be 0.010 min^{-1}, the complex accelerates the GTP hydrolysis rate of RalA by 280,000-fold. These kinetic values are within an order of magnitude of those reported for other GAPs (30, 31).

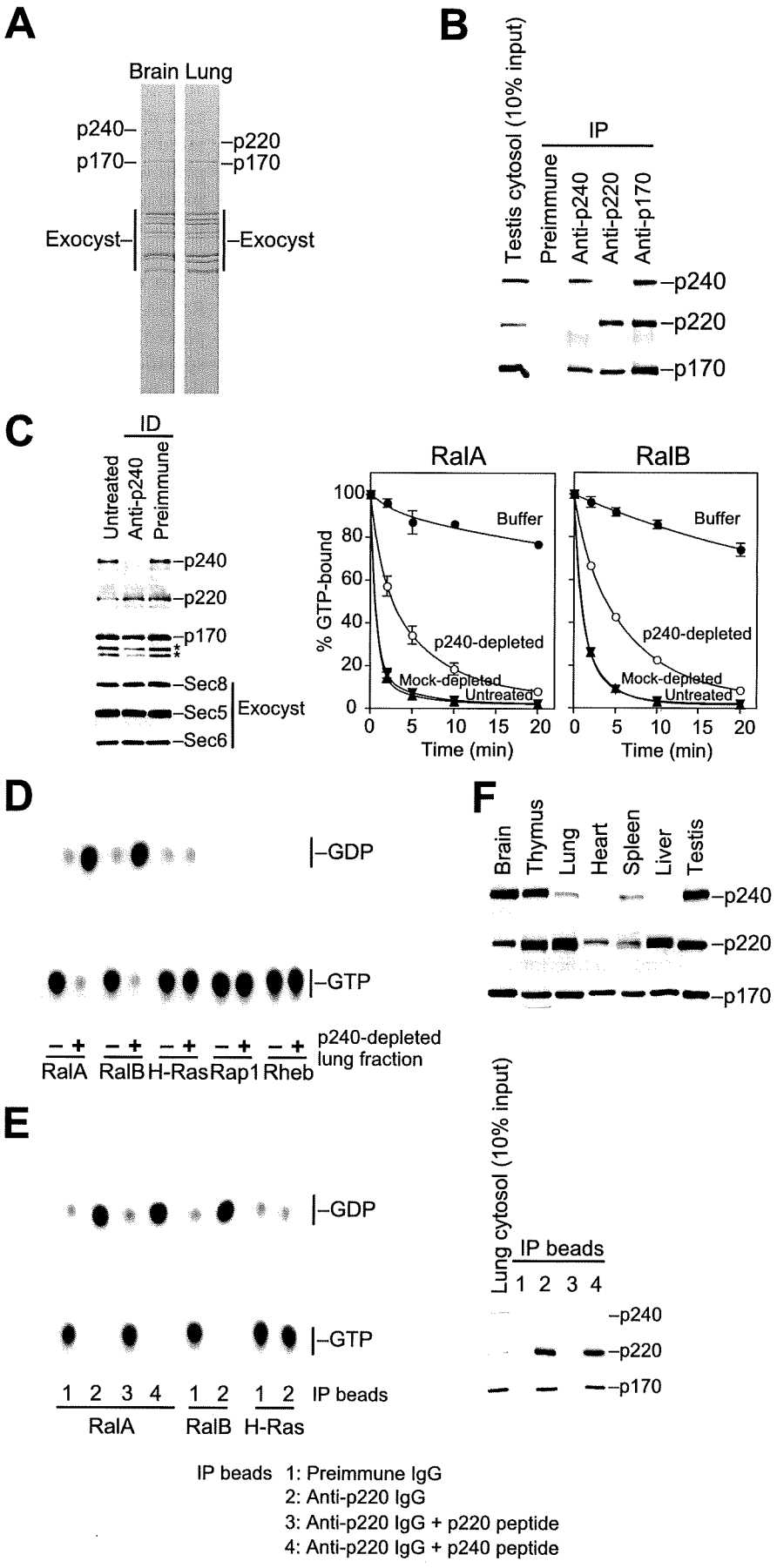

Identification of RalGAPs

We next tested whether dimerization with p170 is required for p240 GAP activity. As shown in Fig. 2*D*, p240 alone had no detectable GAP activity. However, the addition of equimolar p170 to the reaction dramatically enhanced the activity to an extent comparable with that achieved by the complex (Fig. 2*D*). Because p170 alone had no effect on the GTPase activity even at the high concentration (200 nM; Fig. 2*D*), this result indicates that p240 requires p170 for its GAP activity.

Most GAPs, including RasGAPs and RhoGAPs, supply an arginine residue, called the "arginine finger," into the active site of the GTPase to directly catalyze GTP hydrolysis (1). RapGAPs and TSC2 differ from these GAPs in that they do not possess a catalytic arginine but instead use an asparagine residue, termed the "asparagine thumb," for catalysis (39–41). Sequence comparison suggested that p240 also employs the asparagine thumb machinery (supplemental Fig. 1*A*). To test this we mutated the corresponding asparagine of p240 to lysine, which mimics a disease-causing mutation in TSC2 (42), and asked whether this mutant p240^{N1950K} retained RalGAP activity. Although the mutation did not affect the ability of p240 to interact with p170 (data not shown), the p240^{N1950K}-p170 complex showed no appreciable activity for RalA or RalB (Fig. 2*E*). Thus, RalGAP shares the same catalytic mechanism as other asparagine thumb-type GAPs.

Identification of a Second RalGAP Complex from Rat Lung—Tissue distribution analysis revealed that, whereas p170 was abundantly expressed in all rat tissues examined, expression levels of p240 were highly variable between tissues and did not correlate with the p170 expression profile. Specifically, we detected a considerably low level of p240 in the lung (see below). This observation led us to search this tissue for another p170 binding partner that would functionally substitute for p240. To this end, we performed RalA^{Q72L} affinity chromatography with rat lung and brain cytosol. The affinity column eluates were fractionated by gel filtration using the SMART micropurification system, and fractions containing p170 were pooled and analyzed (Fig. 3*A*). We detected similar amounts of p170 and the components of the exocyst complex in both brain and lung fractions (Fig. 3*A*). However, the band intensity of p240 was much weaker in the lung fraction compared with that in the brain fraction (Fig. 3*A*). Instead, a protein of 220 kDa (p220) was detected (Fig. 3*A*). Mass spectrometry analysis identified p220 as the rat orthologue of human C20orf74 (also known as AS250 (43) or KIAA1272). The overall structure of p220 is very similar to p240 (54% amino acid identity); in particular, the C-terminal ~200-amino acid region of p220 shows striking homology to the catalytic region of p240 (85% identity; supplemental Fig. 2*A*). This structural similarity and the fact that p220 was purified as a RalA^{Q72L}-binding protein strongly suggested that p220 also acts as RalGAP, likely as a complex with p170. Using an anti-p220 antibody, we confirmed that p220 immunoprecipitated with p170 from rat testis cytosol (Fig. 3*B*). Importantly, p220 was not co-purified with p240 by either the anti-p220 or p240 antibodies (Fig. 3*B*). This result indicates that the p220-p170 complex is physically distinct from the p240-p170 complex.

To determine whether the p220-p170 complex possesses RalGAP activity, we immunodepleted p240 (and p170 complexed to p240) from the pooled lung fraction with the antibody specific to p240 and then examined the activity remaining in this immunodepleted fraction. The p240-depleted fraction, which contained only the p220-p170 complex and the exocyst complex (Fig. 3*C*, *left*), still exhibited substantial GAP activity, albeit less efficiently than mock-depleted or untreated fractions (Fig. 3*C*, *right*). This residual activity was highly specific for RalA and RalB (Fig. 3*D*). Because the exocyst complex had no effect on Ral GTPase activity (Fig. 1*B*), these results suggest that the p220-p170 complex also has RalGAP activity. To more directly examine the activity of the p220-p170 complex, we tested the activity of the complex immunoprecipitated with the p220-specific peptide antibody. The p220 immunoprecipitates prepared from rat lung cytosol, which also contained p170 but were devoid of p240 (Fig. 3*E*, *right*), exhibited Ral-specific GAP activity (Fig. 3*E*, *left*). When immunoprecipitates were prepared in the presence of excess p220 antigen peptide, the activity of the immunoprecipitates disappeared completely (Fig. 3*E*). This result indicates that the p220-p170 complex actually has specific GAP activity for Ral GTPases. Consistent with its role as a second RalGAP catalytic subunit, p220 is abundantly expressed in tissues where p240 expression levels are relatively low, such as the lung and liver (Fig. 3*F*). Thus, there exist the two structurally similar catalytic subunits, p240 and p220, with complementary tissue expression patterns.

p170 Knockdown Leads to Sustained Activation of RalA in EGF-stimulated PC12 Cells—Finally, we performed RNA interference experiments to test whether the two complexes function as RalGAPs in intact cells. Two distinct siRNAs targeting p170, but not scrambled controls, suppressed the levels of p170 expression in PC12 cells (Fig. 4*A*). Suppression of p170 expression also led to the reduction in p240 and p220 levels (Fig. 4*A*), suggesting that p170 contributes to stability of its binding partners. In p170 knockdown cells, RalA existed in a relatively acti-

FIGURE 3. **The p220-p170 complex; a second RalGAP identified from rat lung.** *A*, comparison of RalA^{Q72L}-binding proteins from rat brain and lung cytosol. RalA^{Q72L} affinity column eluates were fractionated by gel filtration, and fractions containing p170 (fractions 17–22) were pooled and analyzed by SDS-PAGE and Coomassie Blue staining. p240, p220, p170, and the components of the exocyst complex are indicated, as identified by Western blotting and mass spectrometry. *B*, co-immunoprecipitation of p220 and p170 from rat testis cytosol. Note that p220 is not co-purified with p240. *IP*, immunoprecipitation. *C*, the pooled lung fraction depleted of p240 retains RalGAP activity. *Left panel*, the pooled lung fraction was treated with anti-p240 IgG- or preimmune IgG-coated beads, and the resulting supernatants were analyzed for the specified proteins. *Asterisks* denote degradation products of p170. *Right graphs*, RalGAP activity of the immunodepleted fractions was measured by the filter-binding assay (mean ± S.E., $n = 2$). *ID*, immunodepletion. *D*, autoradiograph showing that the p240-depleted lung fraction has Ral-specific GAP activity. Ras subfamily GTPases preloaded with [α-^{32}P]GTP were incubated at 30 °C for 10 min with (+) or without (−) the p240-depleted lung fraction. *E*, immunoprecipitates prepared from rat lung cytosol with preimmune IgG (*IP beads 1*), anti-p220 IgG (*IP beads 2*), or anti-p220 IgG absorbed with p220 antigen peptide (*IP beads 3*) or p240 antigen peptide (*IP beads 4*) were used in GTPase assays with the indicated GTPases preloaded with [α-^{32}P]GTP. After 10 min of incubation at 30 °C, bound radiolabeled nucleotides were analyzed by thin layer chromatography and autoradiography. The *right panel* shows Western blot analysis of the immunoprecipitates with the indicated antibodies. *F*, Western blot analysis of p240, p220, and p170 in rat tissues.

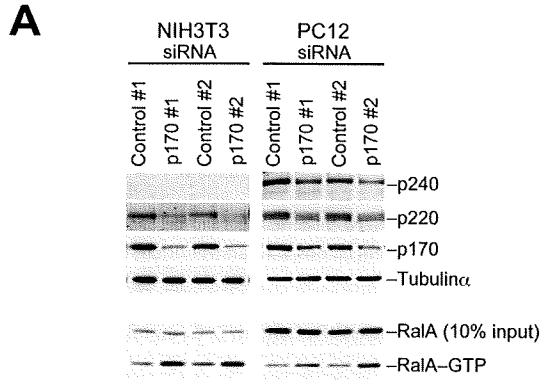

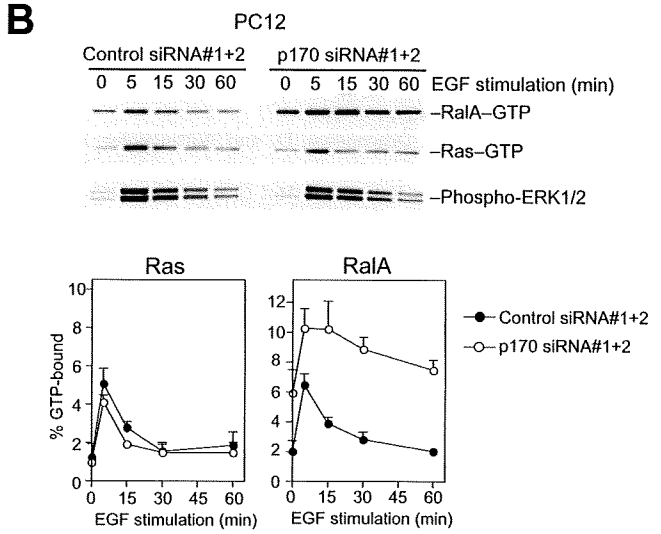

FIGURE 4. **p170 knockdown leads to sustained activation of RalA.** *A*, PC12 or NIH3T3 cells transfected with the indicated siRNAs were lysed, and the levels of the GTP-bound form of RalA (RalA-GTP) were determined by a pull-down assay using Sec5 Ral binding domain as described under "Experimental Procedures." Lysates were also analyzed for the levels of the specified proteins. *B*, PC12 cells transfected with the indicated siRNAs were serum-starved and then stimulated with EGF (20 ng ml^{-1}). At the indicated time points, cells were lysed, and the amounts of RalA-GTP and Ras-GTP in the same lysate were determined. Lysates were also probed for phosphorylated ERK1/2. The *lower graphs* show quantification of Ras-GTP and RalA-GTP levels (means ± S.E., $n = 3$).

vated state with an ~3-fold increase in the GTP-bound form (Fig. 4*A*). We obtained similar results with NIH3T3 cells, which predominantly expressed p220 (Fig. 4*A*). These results indicate that the complexes play a substantial role in maintaining RalA in an inactive state.

We then examined the effects of reducing p170 on the activation/inactivation kinetics of RalA after stimulation with EGF. Many growth factors, including EGF, have been shown to activate RalA through the Ras-RalGEF pathway (44). In control PC12 cells, we observed a transient activation of both Ras and RalA with peak activation at 5 min (Fig. 4*B*). By contrast, in p170 knockdown cells the level of GTP-bound RalA further increased from baseline and remained elevated over 15 min followed by a gradual decline, whereas Ras was rapidly inactivated as in control cells (Fig. 4*B*). Phosphorylation of ERKs, an indicator of the Ras-Raf pathway, was not affected in p170 knockdown cells (Fig. 4*B*). These results demonstrate that p170 knockdown specifically impairs RalGAP activity in the cells and

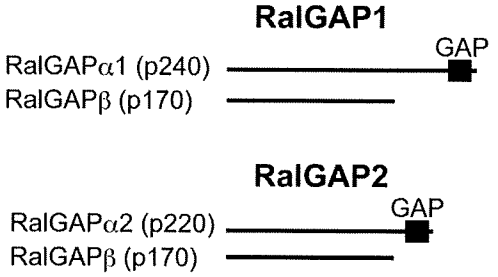

FIGURE 5. **The RalGAP complexes.** Schematic representation of RalGAP1 and RalGAP2. RalGAP1 is composed of the catalytic subunit RalGAPα1 (p240) and the common subunit RalGAPβ (p170). RalGAP2 is composed of the catalytic subunit RalGAPα2 (p220) and the common subunit RalGAPβ (p170).

that the complexes are critical for efficient termination of Ral signaling after growth factor stimulation.

On the basis of these findings, we define the RalGAP complexes as RalGAP1, composed of the catalytic subunit RalGAPα1 (p240) and the common subunit RalGAPβ (p170), and RalGAP2, composed of RalGAPα2 (p220) and RalGAPβ (p170) (Fig. 5). RalGAPα1 and -α2 along with their relatives TSC2 and RapGAPs define a distinct family of GAPs that use a catalytic asparagine (supplemental Fig. 1*B*). Both catalytic and common subunits are highly conserved from fly to mammals, which suggests that the heterodimeric structure of RalGAP is strictly conserved across species (supplemental Fig. 2). Heterodimer dissociation may be involved in the regulation of GAP activity, as shown for the TSC2-TSC1 complex (45–47).

Increasing evidence indicates that Ral GTPases play crucial roles in tumor cell growth (10–13), survival (10, 14), and metastasis (12, 48). A recent *in vivo* study showing that mice deficient for RalGDS, the founding member of the Ras-regulated RalGEFs, are resistant to Ras-mediated skin carcinogenesis (49) further supports the role for Ral activation in Ras-induced tumorigenesis. Our identification of RalGAPs now allows investigation into the biological roles of negative regulation of Ral signaling. Considering the aberrant activation of Ral GTPases in many human cancer tissues (12, 50), it is possible that RalGAP function is impaired in human cancers.

Acknowledgments—We are grateful to the KAZUSA DNA Research Institute for providing the KIAA1219 clone. We thank T. Matsubara for technical assistance.

REFERENCES

1. Bos, J. L., Rehmann, H., and Wittinghofer, A. (2007) *Cell* **129,** 865–877
2. Feig, L. A. (2003) *Trends Cell Biol.* **13,** 419–425
3. Camonis, J. H., and White, M. A. (2005) *Trends Cell Biol.* **15,** 327–332
4. Bodemann, B. O., and White, M. A. (2008) *Nat. Rev. Cancer* **8,** 133–140
5. Brymora, A., Valova, V. A., Larsen, M. R., Roufogalis, B. D., and Robinson, P. J. (2001) *J. Biol. Chem.* **276,** 29792–29797
6. Moskalenko, S., Henry, D. O., Rosse, C., Mirey, G., Camonis, J. H., and White, M. A. (2002) *Nat. Cell Biol.* **4,** 66–72
7. Sugihara, K., Asano, S., Tanaka, K., Iwamatsu, A., Okawa, K., and Ohta, Y. (2002) *Nat. Cell Biol.* **4,** 73–78
8. Cantor, S. B., Urano, T., and Feig, L. A. (1995) *Mol. Cell. Biol.* **15,** 4578–4584
9. Jullien-Flores, V., Dorseuil, O., Romero, F., Letourneur, F., Saragosti, S., Berger, R., Tavitian, A., Gacon, G., and Camonis, J. H. (1995) *J. Biol. Chem.* **270,** 22473–22477
10. Chien, Y., and White, M. A. (2003) *EMBO Rep.* **4,** 800–806

11. Lim, K. H., Baines, A. T., Fiordalisi, J. J., Shipitsin, M., Feig, L. A., Cox, A. D., Der, C. J., and Counter, C. M. (2005) *Cancer cell* **7,** 533–545
12. Lim, K. H., O'Hayer, K., Adam, S. J., Kendall, S. D., Campbell, P. M., Der, C. J., and Counter, C. M. (2006) *Curr. Biol.* **16,** 2385–2394
13. Sablina, A. A., Chen, W., Arroyo, J. D., Corral, L., Hector, M., Bulmer, S. E., DeCaprio, J. A., and Hahn, W. C. (2007) *Cell* **129,** 969–982
14. Chien, Y., Kim, S., Bumeister, R., Loo, Y. M., Kwon, S. W., Johnson, C. L., Balakireva, M. G., Romeo, Y., Kopelovich, L., Gale, M., Jr., Yeaman, C., Camonis, J. H., Zhao, Y., and White, M. A. (2006) *Cell* **127,** 157–170
15. Albright, C. F., Giddings, B. W., Liu, J., Vito, M., and Weinberg, R. A. (1993) *EMBO J.* **12,** 339–347
16. Kikuchi, A., Demo, S. D., Ye, Z. H., Chen, Y. W., and Williams, L. T. (1994) *Mol. Cell. Biol.* **14,** 7483–7491
17. Wolthuis, R. M., Bauer, B., van 't Veer, L. J., de Vries-Smits, A. M., Cool, R. H., Spaargaren, M., Wittinghofer, A., Burgering, B. M., and Bos, J. L. (1996) *Oncogene* **13,** 353–362
18. Shao, H., and Andres, D. A. (2000) *J. Biol. Chem.* **275,** 26914–26924
19. Urano, T., Emkey, R., and Feig, L. A. (1996) *EMBO J.* **15,** 810–816
20. Wolthuis, R. M., de Ruiter, N. D., Cool, R. H., and Bos, J. L. (1997) *EMBO J.* **16,** 6748–6761
21. Rebhun, J. F., Chen, H., and Quilliam, L. A. (2000) *J. Biol. Chem.* **275,** 13406–13410
22. de Bruyn, K. M., de Rooij, J., Wolthuis, R. M., Rehmann, H., Wesenbeek, J., Cool, R. H., Wittinghofer, A. H., and Bos, J. L. (2000) *J. Biol. Chem.* **275,** 29761–29766
23. Ceriani, M., Scandiuzzi, C., Amigoni, L., Tisi, R., Berruti, G., and Martegani, E. (2007) *Exp. Cell Res.* **313,** 2293–2307
24. Hamad, N. M., Elconin, J. H., Karnoub, A. E., Bai, W., Rich, J. N., Abraham, R. T., Der, C. J., and Counter, C. M. (2002) *Genes Dev.* **16,** 2045–2057
25. Rangarajan, A., Hong, S. J., Gifford, A., and Weinberg, R. A. (2004) *Cancer Cell* **6,** 171–183
26. Emkey, R., Freedman, S., and Feig, L. A. (1991) *J. Biol. Chem.* **266,** 9703–9706
27. Higashi, T., Ikeda, T., Shirakawa, R., Kondo, H., Kawato, M., Horiguchi, M., Okuda, T., Okawa, K., Fukai, S., Nureki, O., Kita, T., and Horiuchi, H. (2008) *J. Biol. Chem.* **283,** 8746–8755
28. Kawato, M., Shirakawa, R., Kondo, H., Higashi, T., Ikeda, T., Okawa, K., Fukai, S., Nureki, O., Kita, T., and Horiuchi, H. (2008) *J. Biol. Chem.* **283,** 166–174
29. Fukai, S., Matern, H. T., Jagath, J. R., Scheller, R. H., and Brunger, A. T. (2003) *EMBO J.* **22,** 3267–3278
30. Gideon, P., John, J., Frech, M., Lautwein, A., Clark, R., Scheffler, J. E., and Wittinghofer, A. (1992) *Mol. Cell. Biol.* **12,** 2050–2056
31. Brownbridge, G. G., Lowe, P. N., Moore, K. J., Skinner, R. H., and Webb, M. R. (1993) *J. Biol. Chem.* **268,** 10914–10919
32. Schwarzbraun, T., Vincent, J. B., Schumacher, A., Geschwind, D. H., Oliveira, J., Windpassinger, C., Ofner, L., Ledinegg, M. K., Kroisel, P. M., Wagner, K., and Petek, E. (2004) *Genomics* **84,** 577–586
33. Castro, A. F., Rebhun, J. F., Clark, G. J., and Quilliam, L. A. (2003) *J. Biol. Chem.* **278,** 32493–32496
34. Garami, A., Zwartkruis, F. J., Nobukuni, T., Joaquin, M., Roccio, M., Stocker, H., Kozma, S. C., Hafen, E., Bos, J. L., and Thomas, G. (2003) *Mol. Cell* **11,** 1457–1466
35. Inoki, K., Li, Y., Xu, T., and Guan, K. L. (2003) *Genes Dev.* **17,** 1829–1834
36. Tee, A. R., Manning, B. D., Roux, P. P., Cantley, L. C., and Blenis, J. (2003) *Curr. Biol.* **13,** 1259–1268
37. Zhang, Y., Gao, X., Saucedo, L. J., Ru, B., Edgar, B. A., and Pan, D. (2003) *Nat. Cell Biol.* **5,** 578–581
38. Crino, P. B., Nathanson, K. L., and Henske, E. P. (2006) *N. Engl. J. Med.* **355,** 1345–1356
39. Daumke, O., Weyand, M., Chakrabarti, P. P., Vetter, I. R., and Wittinghofer, A. (2004) *Nature* **429,** 197–201
40. Scrima, A., Thomas, C., Deaconescu, D., and Wittinghofer, A. (2008) *EMBO J.* **27,** 1145–1153
41. Li, Y., Inoki, K., and Guan, K. L. (2004) *Mol. Cell. Biol.* **24,** 7965–7975
42. Maheshwar, M. M., Cheadle, J. P., Jones, A. C., Myring, J., Fryer, A. E., Harris, P. C., and Sampson, J. R. (1997) *Hum. Mol. Genet.* **6,** 1991–1996
43. Gridley, S., Chavez, J. A., Lane, W. S., and Lienhard, G. E. (2006) *Cell. Signal.* **18,** 1626–1632
44. Wolthuis, R. M., Zwartkruis, F., Moen, T. C., and Bos, J. L. (1998) *Curr. Biol.* **8,** 471–474
45. Inoki, K., Li, Y., Zhu, T., Wu, J., and Guan, K. L. (2002) *Nat. Cell Biol.* **4,** 648–657
46. Potter, C. J., Pedraza, L. G., and Xu, T. (2002) *Nat. Cell Biol.* **4,** 658–665
47. Cai, S. L., Tee, A. R., Short, J. D., Bergeron, J. M., Kim, J., Shen, J., Guo, R., Johnson, C. L., Kiguchi, K., and Walker, C. L. (2006) *J. Cell Biol.* **173,** 279–289
48. Yin, J., Pollock, C., Tracy, K., Chock, M., Martin, P., Oberst, M., and Kelly, K. (2007) *Mol. Cell. Biol.* **27,** 7538–7550
49. González-García, A., Pritchard, C. A., Paterson, H. F., Mavria, G., Stamp, G., and Marshall, C. J. (2005) *Cancer Cell* **7,** 219–226
50. Smith, S. C., Oxford, G., Baras, A. S., Owens, C., Havaleshko, D., Brautigan, D. L., Safo, M. K., and Theodorescu, D. (2007) *Clin. Cancer Res.* **13,** 3803–3813

THE JOURNAL OF BIOLOGICAL CHEMISTRY VOL. 285, NO. 7, pp. 4920–4930, February 12, 2010

MicroRNA-15b Modulates Cellular ATP Levels and Degenerates Mitochondria via Arl2 in Neonatal Rat Cardiac Myocytes*[S]

Received for publication, November 5, 2009 Published, JBC Papers in Press, December 10, 2009, DOI 10.1074/jbc.M109.082610

Hitoo Nishi[‡], Koh Ono[‡1], Yoshitaka Iwanaga[§], Takahiro Horie[‡], Kazuya Nagao[‡], Genzou Takemura[¶], Minako Kinoshita[‡], Yasuhide Kuwabara[‡], Rieko Takanabe Mori[‖], Koji Hasegawa[‖], Toru Kita[‡], and Takeshi Kimura[‡]

From the [‡]Department of Cardiovascular Medicine, Graduate School of Medicine, Kyoto University, Kyoto 606-8507, the [§]Division of Cardiology, Department of Internal Medicine, Kinki University School of Medicine, Osakasayama 589-8511, the [¶]Division of Cardiology, Gifu University Graduate School of Medicine, Gifu 501-1194, and the [‖]Division of Translational Research, Kyoto Medical Center, National Hospital Organization, Kyoto 612-8555, Japan

MicroRNAs (miRNAs or miRs) are small, non-coding RNAs that modulate mRNA stability and post-transcriptional translation. A growing body of evidence indicates that specific miRNAs can affect the cellular function of cardiomyocytes. In the present study, miRNAs that are highly expressed in the heart were overexpressed in neonatal rat ventricular myocytes, and cellular ATP levels were assessed. As a result, miR-15b, -16, -195, and -424, which have the same seed sequence, the most critical determinant of miRNA targeting, decreased cellular ATP levels. These results suggest that these miRNAs could specifically down-regulate the same target genes and consequently decrease cellular ATP levels. Through a bioinformatics approach, ADP-ribosylation factor-like 2 (Arl2) was identified as a potential target of miR-15b. It has already been shown that Arl2 localizes to adenine nucleotide transporter 1, the exchanger of ADP/ATP in mitochondria. Overexpression of miR-15b, -16, -195, and -424 suppressed the activity of a luciferase reporter construct fused with the 3′-untranslated region of Arl2. In addition, miR-15b overexpression decreased Arl2 mRNA and protein expression levels. The effects of Arl2 siRNA on cellular ATP levels were the same as those of miR-15b, and the expression of Arl2 could restore ATP levels reduced by miR-15b. A loss-of-function study of miR-15b resulted in increased Arl2 protein and cellular ATP levels. Electron microscopic analysis revealed that mitochondria became degenerated in cardiomyocytes that had been transduced with miR-15b and Arl2 siRNA. The present results suggest that miR-15b may decrease mitochondrial integrity by targeting Arl2 in the heart.

MicroRNAs (miRNAs or miRs)[2] are small, non-coding RNAs that modulate mRNA stability and post-transcriptional translation. A growing body of evidence indicates that miRNAs are involved in basic cell functions, including early development and oncogenesis. In the heart, microarray analysis has shown that the expression profile of miRNAs is altered in human heart disease and animal models of cardiac hypertrophy or heart failure (1–3). Numerous studies have revealed that various subcellular organelles, such as the extracellular matrix, myofibrils, sarcoplasmic reticulum, nucleus, and mitochondria, undergo various changes in biochemical composition and structure in cardiac diseases (4–8, 10, 11). These findings imply an association between miRNAs and subcellular organelles, and the identification of the miRNAs and their target genes that affect subcellular organelles may lead to new understandings in cardiac pathophysiology.

The present study focused on the relationship in cardiomyocytes between specific miRNAs, cellular ATP levels, and mitochondria, which are highly abundant and constitute ~40% of the total cardiomyocyte volume in the heart (9) and mostly generate cellular ATP. To identify miRNAs that can affect cellular ATP levels and mitochondria, the cellular ATP levels of cardiac myocytes, in which a specific miRNA was overexpressed, were assessed. A series of highly expressed miRNAs in the heart were individually overexpressed in neonatal rat cardiomyocytes using a lentiviral vector, and miR-15b was found to decrease cellular ATP levels without affecting cell viability. miR-16, -195, and -424, which have the same seed sequence as miR-15b, also decreased cellular ATP levels. Seed sequences are arranged between the second and eighth nucleotides of the sequence of miRNAs and are the most critical determinant of miRNA targeting (12). Therefore, it was hypothesized that these miRNAs could down-regulate the same target genes and consequently decrease cellular ATP levels.

First we screened a combination of bioinformatics tools for miRNA target prediction, including Target Scan™, Pic Tar™, and MicroCosm™, and found that ADP-ribosylation factor-like 2 (Arl2) was a potential target of these miRNAs that may be

* This work was supported in part by a grant-in-aid for scientific research from the Ministry of Education, Culture, Sports, Science, and Technology of Japan (to K. O., K. H., T. K., and T. K.) and by Grant R31-10069 (WCU Program) from the National Research Foundation of Korea funded by the Ministry of Education, Science, and Technology.

[S] The on-line version of this article (available at http://www.jbc.org) contains supplemental Fig. S1–S4.

[1] To whom correspondence should be addressed: Dept. of Cardiovascular Medicine, Kyoto University, 54 Shogoin-Kawaharacho, Sakyo-ku, Kyoto 606-8507, Japan. Fax: 81-75-751-3203; E-mail: kohono@kuhp.kyoto-u.ac.jp.

[2] The abbreviations used are: miRNA or miR, microRNA; ANT1, adenine nucleotide transporter 1; Arl2, ADP ribosylation factor-like 2; BART, Binder of Arl2; Bcl-2, B-cell CLL/lymphoma 2; EmGFP, emerald green fluorescent protein; siRNA, small interfering RNA; Luc, luciferase; NRVM, neonatal ventricular myocyte; UTR, untranslated region; GAPDH, glyceraldehyde-3-phosphate dehydrogenase; Bis-Tris, 2-[bis(2-hydroxyethyl)amino]-2-(hydroxymethyl)propane-1,3-diol; PBS, phosphate-buffered saline; wt, wild type; mut, mutant.

directly associated with cellular ATP and mitochondria. Arl2 is notable for several unusual features within the ADP-ribosylation factor (Arf) family, including the apparent lack of N-terminal myristoylation, rapid and phospholipid-independent binding of GTP, and association with mitochondria (13, 14). Arl2 forms a complex with Binder of Arl2 (BART), an Arl2-specific effector, and localizes with adenine nucleotide transporter 1 (ANT1) (13). ANT exchanges matrix ATP for cytosolic ADP across the inner mitochondrial membrane and plays a central role in oxidative phosphorylation (15).

The present study shows that 1) miR-15b, -16, -195, and -424, which have the same seed sequence, reduced ATP levels in neonatal cardiac myocytes, 2) miR-15b controls ATP levels by targeting Arl2 in cardiac myocytes, and 3) miR-15b overexpression and Arl2 knockdown changed the mitochondrial morphology.

EXPERIMENTAL PROCEDURES

Cell Culture—Neonatal rat ventricular myocytes (NRVMs) were isolated from 1-day-old Sprague-Dawley rats as described previously (16). These cells were cultured in Dulbecco's modified Eagle's medium supplemented with 10% fetal bovine serum and 1% penicillin/streptomycin and plated in MULTI-WELL™ PRIMARIA™ 6-well or 24-well plates (BD Biosciences) or Lab-Tek™ chamber slides in 37 °C in a 5% CO_2 incubator. DNA transduction was carried out 48 h after the cells were plated.

Plasmids—miRNA-expressing vectors were constructed using a BLOCK-iT™ Pol II miR RNAi Expression Vector kit (Invitrogen) according to the manufacturer's instructions. Let-7d, miR-1, -15b, -16, -21, -22, -23a, -27a, -29a, -125a, -126–3p, -133a, -133b, -143, -144, -146, -149, -155, -181, -195, -199a, -214, and -424 expression plasmids were made. A control miRNA-expressing vector (miR-cont.) was obtained from the kit. For the construction of anti-miR-15b, double-stranded oligonucleotides containing three or six tandem sequences that were completely complementary to miR-15b were inserted into a pMIR-REPORT™ vector (Ambion) at the PmeI site (Luc-15b decoy). EmGFP-miR-15b decoy was constructed by replacing the luciferase gene with an EmGFP gene. siRNA vectors were constructed from pSINsi-mU6 DNA™ (Takara Bio). Double-stranded oligonucleotides were inserted into pSINsi-mU6 DNA™ at BamHI/ClaI sites. The oligonucleotides that targeted specific genes and scrambled control (scrambled siRNA) were as follows: Arl2 (5′-GGATTCAAGCTGAACATCT-3′ (Arl2 siRNA1) and 5′-CTGACCATTCTGAAGAAGA-3′ (Arl2 siRNA2)); Bcl-2 (5′-GAGATCGTGATGAAGTACA-3′ (Bcl-2 siRNA1) and 5′-GGATGACTGAGTACCTGAA-3′ (Bcl-2 siRNA2)); BART (5′-CGCTGGCGACATCTTTGAC-3′ (BART siRNA1) and 5′ -CGCTTCCCAGAACAACCTA-3′ (BART siRNA2)); Scrambled control (5′-AATAATAATGGG-GGGATCC-3′. All of these constructs were inserted into a pLenti6/V5-D-TOPO™ vector (Invitrogen). The rat Arl2 gene was amplified and cloned into a pLenti6/V5-D-TOPO vector using the following primers: forward (5′-CACCATGGGGCT-TCTGACCATTCT-3′) and reverse (5′-TCAGTCGGCAGTA-AAGACAC-3′). The following primers were used to amplify and clone the 3′-UTR of the mouse Arl2 gene into a pMIR-REPORT™ luciferase vector at the SpeI/HindIII sites (Arl2–3′-UTR Luc) according to the manufacturer's instructions: forward (5′-GGACTAGTGCTTCTTCAGTGTCCCCAGG-3′) and reverse (5′-CCCAAGCTTGTGAAGAGTGCTTTAT-TCT-3′). The forward primer included a SpeI restriction site, and the reverse primer had a HindIII site (underlined).

Lentivirus Production and DNA Transduction—Lentiviral stocks were produced in 293FT cells according to the manufacturer's protocol (Invitrogen). In brief, virus-containing medium was collected 48 h post-transfection and filtered through a 0.45-μm filter. One round of lentiviral infection was performed by replacing the medium with virus-containing medium that contained 8 μg/ml Polybrene followed by centrifugation at 2500 rpm for 30 min at 32 °C.

RNA Extraction, Quantitative Real-time PCR, and Reverse Transcription-PCR—Total RNA was isolated and purified from NRVMs using TRIzol™ reagent (Invitrogen), and cDNA was synthesized from 5 μg of total RNA using SuperScriptII™ reverse transcriptase (Invitrogen) according to the manufacturer's instructions. For quantitative real-time-PCR, specific genes were amplified for 40 cycles using SYBR™ Green PCR Master Mix (Applied Biosystems). Expression was normalized to the housekeeping gene GAPDH. The primers used were as follows: GAPDH, rat forward (5′-TTGCCATCAACGACCCCTTC-3′), human forward (5′-TTGCCATCAATGACCCCTTC-3′), and reverse (5′-TTGTCATGGATGACCTTGGC-3′); Arl2, rat forward (5′-GAAGCAGAAAGAGCGAGA-3′) and reverse (5′-CAGTAAAGACACGACTGGA-3′); Arl2, human forward (5′-GAAGCAGAAAGAGCGGGA-3′) and reverse (5′-CTGT-GAAAATGCGGCTGGA-3′); EmGFP, forward (5′-AGCAA-AGACCCCAACGAGAA-3′) and reverse (5′-GGCGGCGGT-CACGAA-3′). For reverse transcription-PCR, the rat BART gene was amplified for 25 cycles using TaqDNA polymerase (New England Biolabs, Ipswich, MA) according to the manufacturer's instructions with specific primers as follows: BART, forward (5′-ATGGACAAGTACTACCAGGA-3′) and reverse (5′-CTTACACAGAGAAGTCACCA-3′). The 318-bp fragment was electrophoresed on 1.5% agarose gels and stained using SYBR™ Green I (Invitrogen).

Electron Microscopy—NRVMs on 6-well plates were fixed overnight in phosphate-buffered 2.5% glutaraldehyde (pH 7.4) and then post-fixed for 1 h in 1% osmium tetroxide. The samples were then prepared conventionally for transmission electron microscopy (H-800, Hitachi). We performed a morphometric analysis under an electron microscope using the method described previously with some modification (17). In brief, a uniform sampling of 10 electron micrographs was used for the morphometric assay of each group. Five random fields micrographed at 20,000× from each of five blocks were printed at a final magnification of 50,000× and analyzed on composite grids as described previously to calculate the density of mitochondria (number/μm^2), the percentage of shrunken or degenerated mitochondria (%), and the size of mitochondria (μm^2) within a cardiomyocyte.

Measurement of Cellular ATP—The amount of ATP in the cell lysates was measured using a luciferin-luciferase ATP assay system (Toyo Ink Co.) in accordance with the manufacturer's instructions. Genomic DNA or protein was extracted from the

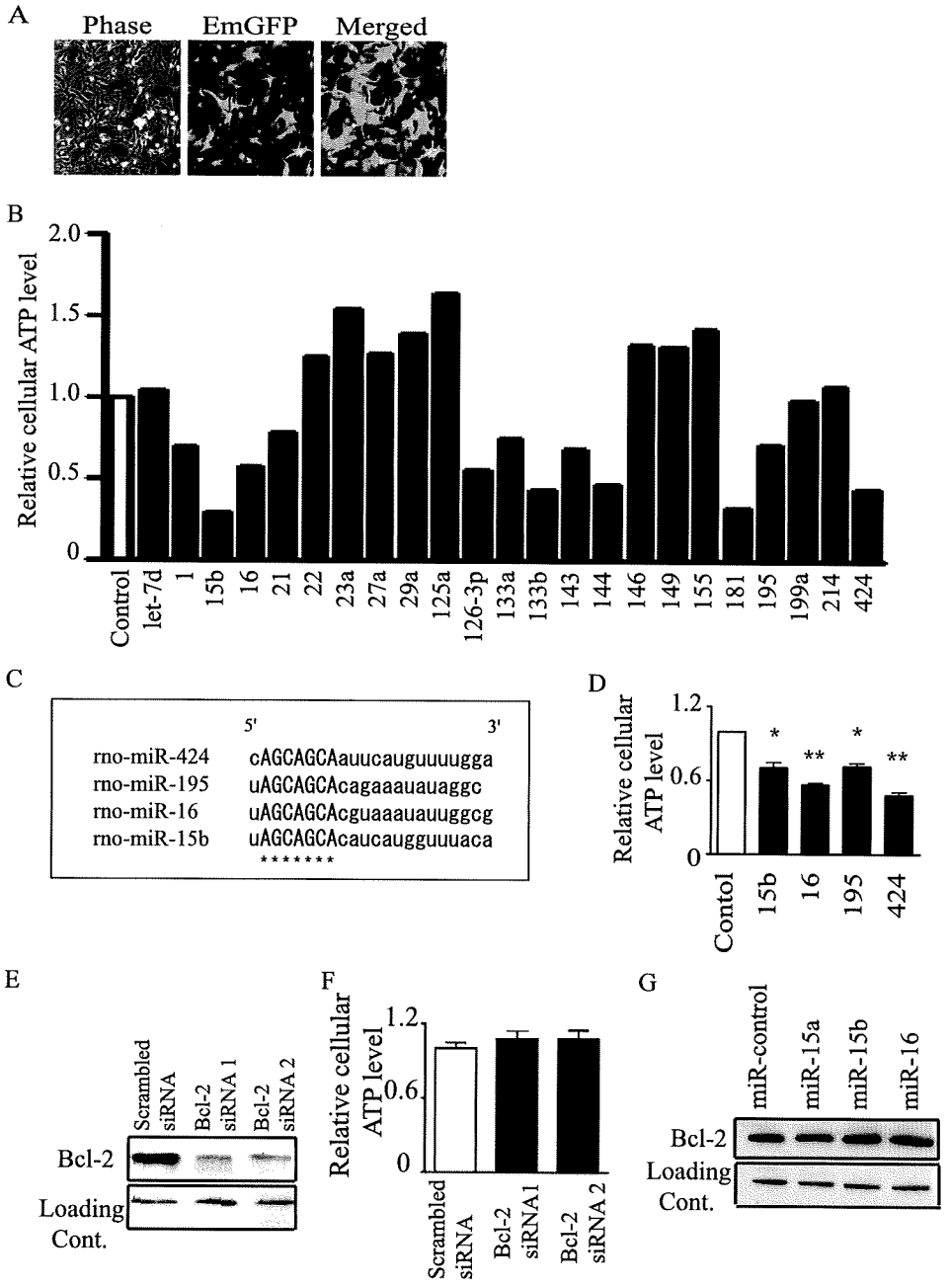

FIGURE 1. **miR-15b, -16, -195, and -424 decrease cellular ATP levels.** *A*, shown is expression of the EmGFP gene in NRVMs. *B*, cellular ATP levels of miR-control or individual miRNAs overexpressing NRVMs 72 h after transduction by a lentiviral vector in serum-containing medium are shown. *C*, structure of the mature forms of miR-15b, -16, -195, and -424 is shown. The sequence marked by *asterisks* is the seed sequence. *D*, cellular ATP levels of miR-control or miR-15b, -16, -195, and -424 overexpressing NRVMs 72 h after transduction by a lentiviral vector in serum-containing medium are shown. *E* and *F*, immunoblots of Bcl-2 (*E*) and cellular ATP levels (*F*) in NRVMs transduced with Bcl-2 siRNAs are shown. *G*, immunoblots of Bcl-2 in NRVMs transduced with miR-15 and -16 are shown. The *bar graph* indicates values expressed as relative ATP levels compared with that of miR-control (*D*) or scrambled siRNA (*F*). In *D* and *F*, data are presented as the mean ± S.E. of three independent experiments (*, $p < 0.05$; **, $p < 0.01$ *versus* control).

same samples as used for the ATP assay, and the amount of DNA or protein was used to normalize the cell number.

Cell Viability—Total lactate dehydrogenase activity in the culture medium was measured using a lactate dehydrogenase Cytotoxicity Assay Kit™ (Cayman Chemical Co.) in accordance with the manufacturer's instructions. The values were standardized to the amount of protein extracted from the same samples. Viable or dead cells were determined by calcein AM or ethidium homodimer (EthD-1) dyes, respectively, using a LIVE/DEAD™ Viability/Cytotoxicity kit (Invitrogen). Five random fields, micrographed at 20×, from each well were printed, and the numbers of viable and dead cells were counted and calculated to give the percentages of each cell group.

Luciferase Assay—For luciferase reporter assays, constructs were transiently transfected into 293FT cells using FuGENE 6™ (Roche Applied Science) or into NRVMs using Lipofectamine 2000™ (Invitrogen) at the following concentrations: 0.1 μg of firefly luciferase reporter gene (Arl2–3′-UTR Luc or Luc-miR-15b decoy), 0.01 μg of pRL-TK™ Renilla reniformis luciferase control plasmid (Promega), and 0.1 μg of BLOCK-iT Pol II miR RNAi Expression Vector encoding the appropriate miRNA or the control. At 24 h after transfection, both luciferase activities were measured using a dual luciferase reporter assay system (Toyo Ink Co.). Firefly luciferase activity was normalized for transfection efficiency by measuring Renilla reniformis luciferase control activity according to the manufacturer's instructions.

Western Immunoblotting Analysis—Immunoblotting analysis was performed using standard procedures as described previously (18). Cultured cells were homogenized in lysis buffer consisting of 100 mM Tris-HCl, pH 7.4, 75 mM NaCl, and 1% Triton™ X-100 (Nacalai Tesque). The buffer was supplemented with Complete Mini™ protease inhibitor (Roche Applied Science), 0.5 mM NaF, and 10 μM Na_3VO_4 just before use. The protein concentration was determined using a BCA protein assay kit (Bio-Rad). A total of 50 μg of protein was fractionated using NUPAGE™ 4–12% Bis-Tris (Invitrogen) gels and transferred to a PROTRAN™ nitrocellulose transfer membrane (Whatman). The membrane was blocked using 1× PBS containing 5% nonfat milk for 1 h and incubated with the primary antibody overnight at 4 °C. After being washed in 0.05% T-PBS (1×PBS and 0.05% Tween 20), the membrane was incubated with the secondary antibody for 1 h at 4 °C. After the membrane was washed again in 0.05% T-PBS, the immune complexes were detected using

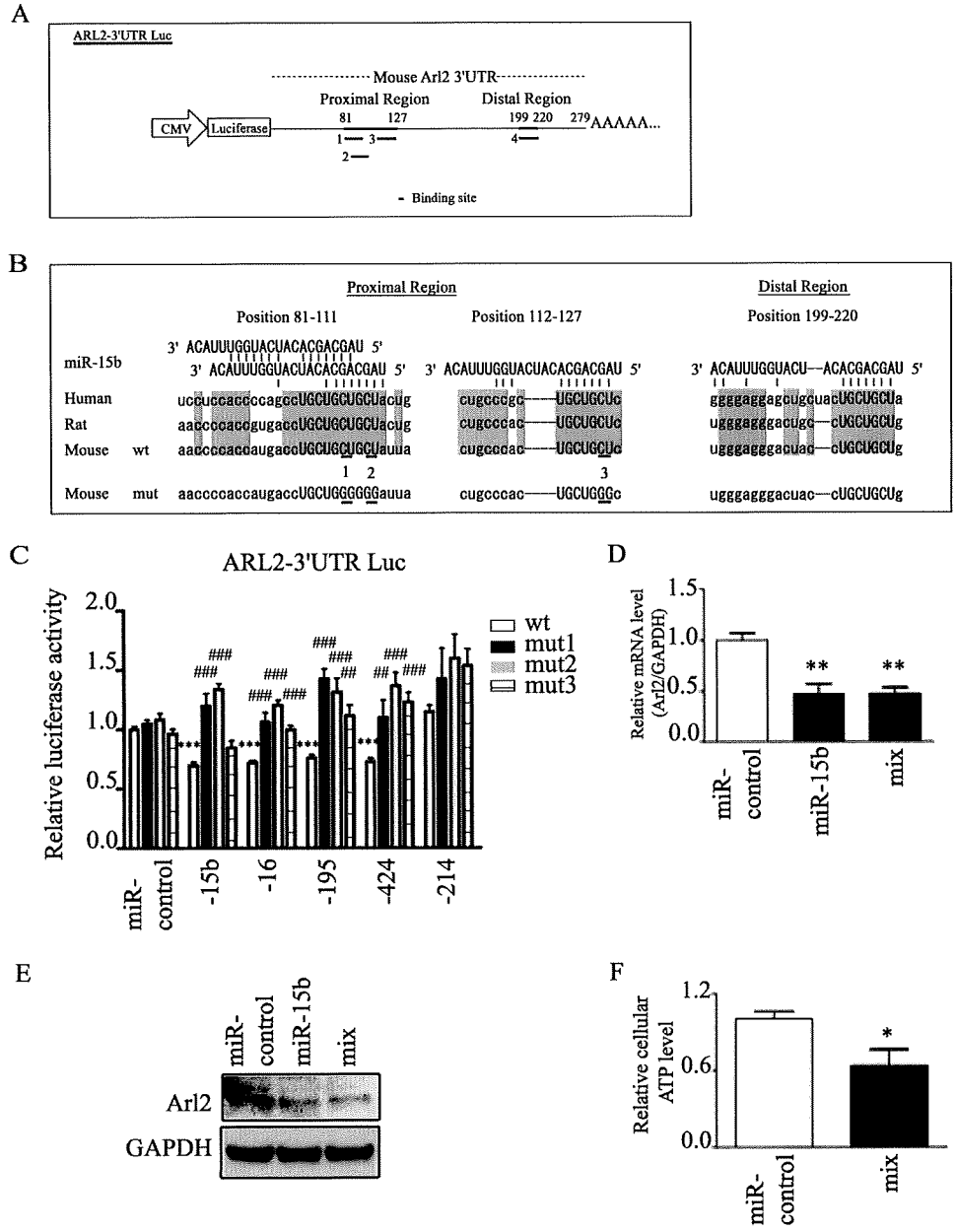

FIGURE 2. **miR-15b targets Arl2.** *A* and *B*, shown is the structure of wild-type- or mutated-Arl2 3′-UTR luciferase construct (wt/mut-Arl2–3′-UTR Luc). The mouse Arl2 3′-UTR was predicted to contain four binding sites of miR-15b, -16, -195, and -424 by TargetScan™ (*A*). These binding sites are highly conserved among species (*B*). The *gray background* indicates the same sequence between human, rat, and mouse. *C*, 293FT cells were transfected with a wt/mut-Arl2–3′-UTR Luc and expression plasmid for individual miRNAs or miR-control. (***, $p <$ 0.001 *versus* wt-control; ##, $p < 0.01$; ###, $p < 0.001$ *versus* wt-miR) NRVMs were transduced with miR-15b or miR-control using a lentiviral vector. *D* and *E*, Arl2 mRNA and protein expression levels were detected 72 h after transduction of miR-control, -15b, or a mixture of multiple miRNAs such as miR-15b, -16, -195, and -424 (mix) by quantitative real-time-PCR (*D*) and immunoblotting (*E*), respectively. *F*, cellular ATP levels 72 h after transduction of the mixture or miR-control are shown. In *D* and *F* data are presented as the mean ± S.E. of three independent experiments (*, $p < 0.05$; **, $p < 0.01$ *versus* control).

ECL-plus™ chemiluminescent detection reagent (Amersham Biosciences). The primary antibodies used were: anti-GAPDH (Cell Signaling Technology), 1:1000; anti-Arl2 (Protein Tech Group, Inc.), 1:500; anti-Bcl-2 (Assay Designs, Ann Arbor, MI), 1:1000. As secondary antibodies, anti-rabbit IgG (GE Healthcare) was used at a dilution of 1:2000. Immunoblots were detected using LAS-1000 (FUJI FILM).

Mitochondria Isolation and ANT Activity—Mitochondria were isolated from NRVMs 72 h after transduction with a lentiviral vector. Isolated mitochondria were loaded with ATP, and ADP/ATP exchange was measured after the addition of external ADP as described previously (19). Carboxyatractyloside was purchased from Sigma.

Statistics—Data are presented as the means ± S.E. Statistical comparisons were performed using unpaired two-tailed Student's *t* tests and a one-way analysis of variance with Bonferroni's or Dunnett's post hoc test where appropriate, and a probability value of <0.05 was taken to indicate significance.

RESULTS

Screening of miRNAs That Alter Cellular ATP Levels—First, lentiviral vectors that expressed let-7d, miR-1, -15b, -16, -21, -22, -23a, -27a, -29a, -125a, -126–3p, -133a, -133b, -143, -144, -146, -149, -155, -181, -195, -199a, -214, and -424 were constructed. Most of these miRNAs have been reported to be highly expressed in the heart (3). To identify miRNAs that can affect cellular ATP levels and mitochondria in the heart, these miRNAs were overexpressed in NRVMs using a lentiviral vector, and the cellular ATP levels were compared. The transduction efficiency was always >90% (Fig. 1*A*). The lentiviral vectors of miR-15b and -195 could express miR-15b or -195, respectively, in NRVMs at levels that greatly exceeded those of endogenous miRNAs in the control. Moreover, miR-15b and -195 could be overexpressed at the same time by a mixture of multiple miRNA vectors consisting of miR-15b, -16, -195, and -424 (supplemental Fig. S1). After these miRNAs were screened, we found that some miRNAs changed cellular ATP levels (Fig. 1*B*). Among these, the mechanisms by which miR-15b, -16, -195, and -424 acted on cardiomyocytes were further examined because these miRNAs share a common seed sequence, which is the most critical determinant of miRNA targeting (12). The common seed sequence, which is arranged between the second and eighth nucleotides, is indicated by *asterisks* in Fig. 1*C*. We strongly suspected that miR-15b, -16, -195, and -424 could down-regulate the same target genes, which were specifically involved in the regulation of cellular ATP. Moreover, it has

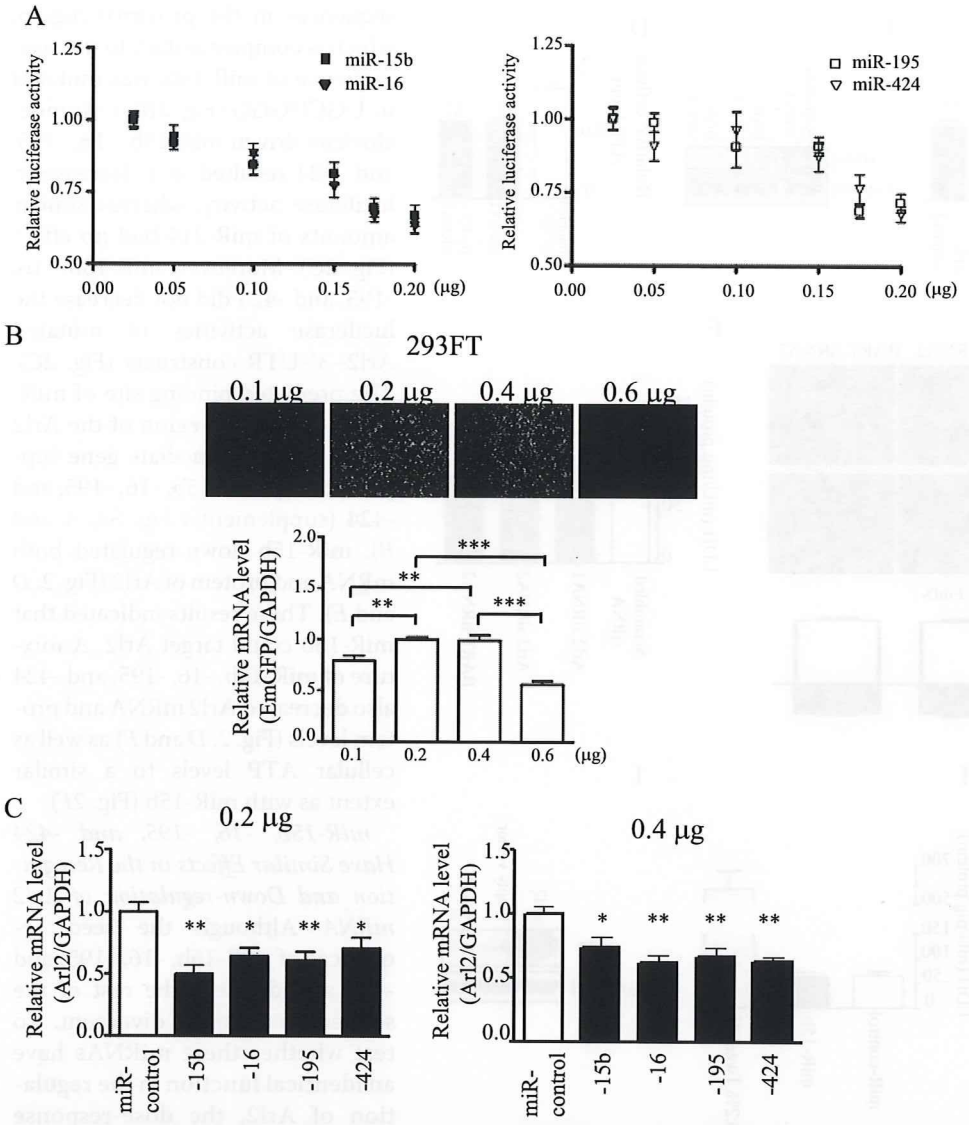

FIGURE 3. **miR-15b, -16, -195, and -424 have similar effects in the recognition and down-regulation of Arl2 mRNA.** *A*, the luciferase activity is shown of Arl2 3′-UTR Luc construct in response to increasing doses of expression plasmids for individual miRNAs ranging from 0.025 to 0.2 μg. The values are luciferase activities relative to that with a dose of 0.025 μg. *B*, the transfection efficacy of expression plasmids for miRNAs at a dose of 0.1, 0.2, 0.4, or 0.6 μg was detected by quantitative real-time-PCR for EmGFP transduced into 293FT cells using Fugene6™. The *bar graph* indicates values expressed as relative EmGFP levels compared with that with a dose of 0.2 μg (**, $p < 0.01$; ***, $p < 0.001$). *C*, mRNA levels are shown of Arl2 in 293FT cells 24 h after transfection with expression plasmids for individual miRNAs at a dose of 0.2 (*left*) and 0.4 μg (*right*). The values are expression levels of Arl2 mRNA relative to that of miR-control. GAPDH was used as an internal control. Data are presented as the mean ± S.E. of three independent experiments (*, $p < 0.05$; **, $p < 0.01$ *versus* control).

been reported that miR-15 and -16 play critical roles in apoptosis of hematopoietic cancer cells (21), and the cardiac-specific overexpression of miR-195 results in cardiac dysfunction *in vivo* (1). Therefore, we considered whether miR-15b, -16, -195, and -424 might play important roles in the heart. In fact, miR-15b, -16, -195, and -424 were found to decrease cellular ATP levels in NRVMs (Fig. 1*D*). A previous study indicated that miR-15 and miR-16 down-regulate Bcl-2, an anti-apoptotic protein, post-transcriptionally in hematopoietic cancer cells (21). Therefore, we examined whether the down-regulation of Bcl-2 could affect cellular ATP levels. Knockdown of Bcl-2 by siRNA did not change cellular ATP levels in NRVMs at 72 h after transduction (Fig. 1, *E* and *F*). Moreover, the overexpression of miR-15 and -16 did not change Bcl-2 protein expression in NRVMs at 72 h after transduction (Fig. 1*G*). These results suggest that other target genes are involved in this ATP reduction by miR-15b, -16, -195, and -424 in NRVMs. Absolute amounts of ATP were also measured. As shown in supplemental Fig. 2, the levels were within an anticipated range (22).

miR-15b Targets Arl2—To identify the targets of miR-15b that modulate cellular ATP levels, we searched for genes that were predicted to be targets of miR-15b by multiple bioinformatics tools for miRNA target prediction, including Target Scan™, Pic Tar™, and MicroCosm™. After this combined screening, 28 genes were picked up as candidates (supplemental Fig. S3*A*). Among these predicted targets of miR-15b, a second search was made for genes for which the function is known to be associated with mitochondria. The six candidates selected were Arl2, glutamate dehydrogenase 1, mitogen-activated protein kinase kinase 1, protein phosphatase 1, regulatory (inhibitor) subunit 11, parathyroid hormone, and TATA box-binding protein. The number of conserved binding sites in their 3′-UTR was then compared. Arl2 had four conserved binding sites, glutamate dehydrogenase 1 and TATA box-binding protein had two sites, and mitogen-activated protein kinase kinase 1, regulatory (inhibitor) subunit 11, and parathyroid hormone had one site according to Target Scan™ (supplemental Fig. S3*B*). Thus, Arl2 was further evaluated as a potential target of miR-15b. Arl2 is a 21-kDa GTPase that forms a complex with BART, an Arl2-specific effector, and localizes to ANT1 (13). ANT exchanges the matrix ATP for cytosolic ADP across the inner mitochondrial membrane and plays a central role in oxidative phosphorylation (15). Therefore, it was hypothesized that miR-15b, -16, -195, and -424 could down-regulate Arl2, which decreases cellular ATP levels via ANT1. Four evolutionarily conserved binding sites of these miRNAs are indicated in Fig. 2*A*. To test whether the putative target sequence in the Arl2 3′-UTR could mediate the repression of Arl2 gene expression, the wild-type or mutated full-length 3′-UTR of the Arl2 transcript was inserted into a luciferase reporter construct (wt/mut Arl2–3′-UTR Luc), which was transfected into 293FT cells. In the mutated luciferase reporter constructs, each of the UGCUGCU